Università
Ca'Foscari
Venezia

Scuola Dottorale di Ateneo
Graduate School
Dottorato di ricerca in Scienze Chimiche
ciclo XXVII
Anno di discussione: 2015

LUMINESCENT DOWN-SHIFTING GLASSES FOR SOLAR APPLICATIONS OBTAINED BY ION EXCHANGE

Settore scientifico disciplinare di afferenza: **CHIM/03**
Tesi di dottorato di **Marco Mardegan** matricola **810696**

Relatore	Coordinatore del Dottorato
Ch.mo Prof. Cattaruzza Elti	Ch.mo Prof. Selva Maurizio

Abstract

To verify the possibility of realizing down-shifting phenomena inside photovoltaic cover glass panels, silicate glasses where doped by ion exchange. Different salt mixtures were compared. The trends obtained from the characterization have been interpreted on the basis of changes in the optical basicity degree along the exchanged layers. A preliminary study is proposed about the relation between the optical basicity degree of the glass and the chemical state of the doping elements. The effectiveness of the improvement of the power produced by a photovoltaic panel covered by the doped glasses was also tested by a home-made system acting as a solar simulator.

Contents

CHAPTER 1

Introduction

Diffusion is one of the most widespread phenomena of mass transport. The term "diffusion" generally means the movement of a substance across a region where a gradient of properties is attained. This is a general concept and examples of this phenomenon can be found in different areas, from physics through chemistry to the biological area: for example, one could refer to all the biological phenomena governed by diffusion until the most abstract concept of the knowledge diffusion. The diffusive phenomena have been widely used for the control of material properties and so evolution technology is somewhat linked to this aspect; in this frame the synthesis technique known as the ion exchange is probably the easiest example of how the diffusion phenomena can be used to modify the materials properties. Nowadays ion exchange has been successfully applied for altering the properties of glasses. The most important application field for ion exchange is photonics for the evolution of optical devices able to control light, as for example the waveguides. Nevertheless it must be considered that the introduction of an element in a matrix could be used to obtain advanced materials for a large class of applications. For example and referring again to the world of glasses, transition metal doped glasses are also studied in the biological area as carriers of medical or disinfectant species. That is only an example of the possibilities allowed by this very simple synthesis technique that in the easiest implementation is realized by dipping the matrix inside a liquid source of the dopant

species required.
This work of thesis is dedicated to silicate glasses doped with transition metals, studied to take advantage from their optical features. More in detail two different studies have been dealt with and the ion exchange is the common thread linking them together. The first topic is related to the study of the matrix influence on the oxidation state of a transition metal (TM). The importance of this study concerns the fact that the final properties of a TM doped glass are the direct consequence of the TM chemical state. In this frame the electron density donor power of the medium, called optical basicity, is of great importance for the TM dopant oxidation state. In the second topic presented the TM doped glasses produced by ion exchange have been studied in relation to the field of photovoltaic energy production. What has been attempted is to take advantage of the doped glasses optical properties to evolve composite materials acting as luminescent down-shifting (LDS) materials for the improvement of the solar cell yield. This means a new optical application field for doped glasses: the photovoltaic area.
Seven chapters compose this dissertation. In the first chapter (introduction) a brief description of diffusion and of the ion exchange techniques are reported. In the second chapter a general introduction to the characterization techniques used is provided as well. The third chapter reports on the preliminary study results about the influences of the matrix characteristics on the oxidation state of the dopant ions introduced by ion exchange. In the fourth part, the preliminary study of application of Cu doped glasses and Ag doped glasses produced by ion exchange as luminescent down-shifting (LDS) materials is proposed. The developments of Ag doped and copper glasses study as LDS has been reported in the fifth and sixth chapter respectively. In the last chapter the results obtained are summarized and some future developments are proposed. Some experimental findings described in the second chapter have been used for the discussion of the results reported in sixth chapter.

1.1 Diffusion: generalities

Diffusion is the movement of atoms or molecules in a material and can occur in a gas, liquid and solid phase too. In the last case diffusion can be figured out as the particles migration (ions or atoms) from lattice point to another one in presence of a chemical potential gradient. Accordingly, the matter diffusion is the main process of solid state reactions i.e. nucleation and growth of new grains, phase separation, etc. Diffusion is not only favored by a gradient of concentration but it is strongly influenced by the temperature (atomic vibrations) and by the presence of defects. The main point is that diffusion can be formalized by mathematical relations making it in principle predictable and that make diffusion one of the most powerful phenomena for changing the material properties. Ion exchange, the synthesis technique used in this work, is based on the migration of atoms in presence of a concentration gradient at high temperature.

1.1.1 I and II Fick's laws

The most general approach for a formal description of the diffusion process is based on the first Fick's law (1.1) that, in the case of one-directional diffusion (along x), is written as

$$J = -D\frac{\partial C}{\partial x} \tag{1.1}$$

where J is diffusing species flux [atoms/m^2s], D the diffusion coefficient or diffusivity [m^2/s] and C the concentration of the diffusing element [atoms/m^3]. The first Fick's law links the atomic flux of particles to the concentration gradient by the diffusivity D that quantifies ease of diffusion of a chemical species; diffusivity is tightly linked to temperature through an Arrhenius-type temperature dependence (1.2)

$$D = D_o \exp(-\frac{Q}{K_B T}) \tag{1.2}$$

where K_B is the Boltzmann's constant [1.38*10^{-23} J/K], T the temperature [K], D_0 is a temperature-independent constant and Q indicates the threshold energy for an atom to break bonds and start to move inside the solid (called activation energy).
In real cases diffusion is a dynamic process because the flux of diffusing

species changes in time; in this situation (and if the diffusivity D does not depend on composition) the second Fick's law (1.3) is verified.

$$\frac{\partial C}{\partial t} = D\frac{\partial^2 C}{\partial x^2} \tag{1.3}$$

From equation 1.3, assuming that the starting concentration of diffusing atoms inside the matrix is constant and equal to C_0 and the concentration at the matrix surface is constant too, it is possible to obtain a relation between local concentration and time (1.4)

$$C_x(t) = C_S - (C_S - C_O)erf\left(\frac{x}{2\sqrt{Dt}}\right) \tag{1.4}$$

where C_x(t) is the concentration of a diffusion species at the time t, at the depth x, and erf(z) is the error function (1.5)

$$erf(z) = \frac{2}{\sqrt{\pi}}\int_0^z e^{(-y)^2}dy \tag{1.5}$$

being

$$z = \frac{x}{2\sqrt{Dt}}. \tag{1.6}$$

The equation 1.4 is a solution of the second Fick's law and it can be used to predict the concentration profile of a diffusing specie inside a matrix. It is worth noting that equation 1.4 can describe the concentration profile only if the conditions assumed for the solution of equation 1.3 are attained; that is true only in a small number of real situations.

1.2 The ion exchange process

The process for which ions under the material surface are replaced by diffusion of an element initially not present inside the material is called ion exchange (IE). This process is based on the diffusion phenomena realized when a matrix is placed in contact with a source of the dopant species. The first characteristic of ion exchange is that it permits to change the matrix composition avoiding the melting of the substrate. For example, referring to the glassy matrices, if a doped glass is prepared by melting the maximum concentration of dopant ions is limited by the solubility point. Differently in ion exchange the mobile ions diffuse inside the solid glass occupying the

lattice points made available by the diffusion of ions initially present inside the matrix; as a consequence, the possible precipitation of the dopant species is negligible, and it is feasible to reach dopant concentrations of the order of 10^{21} atoms/cm^3 [1]. Furthermore, ion exchange makes possible to dope glasses with more than one element by sequential dipping inside different fused salts. All these features make ion exchange one of the most used approaches to introduce elements in a controlled way inside different types of materials for the alteration of the final properties [2].
Ion exchange is not so new as it could be thought: the first examples of ion exchange can be found in the heritage frame. It has been shown that ion exchange was widely used for coloring ancient glass objects [3] and glass luster on ceramics [4] [5]. Nowadays ion exchange is used mainly for technical, industrial and scientific purposes. From the beginning of the twentieth century one of the biggest applications of this technique has been the surface hardening of glass artifacts, usually known as chemical tempering [6] [7] [8] [9]. Subsequently, from the half of the last century until now ion exchange has been successfully applied in the field of photonics because useful to alter the optical properties of a matrix by doping with a specific element. In fact, from the early seventies the ion exchange was mainly studied to realize waveguides and optical switches, devices able to control light in a defined way [10]. Nowadays the application of ion exchange in waveguide production represents the principal application field of this process. Although it has been mainly used to dope glass matrices, there are examples of ion exchange processes realized on $LiNbO_3$ crystals [11] [12] and on organic films too [13]. In the literature examples are present of silicate glasses doped by ion exchange with thallium [14] [15], litium [16], cesium and rubidium [17], erbium [18] [19] [20] [21] and lead [22]. A wide literature exists about the doping with silver or copper. Silver is interesting for the high increment of the matrix refractive index achieved and for the relatively high diffusion coefficient allowing an easy doping. These features make silver one of the most studied elements for the production of waveguides and for studying diffusion inside the glass. The main drawback of silver is its tendency to form metallic nanoparticles. These nanoparticles represent a source of optical losses for a waveguide, but otherwise their formation is studied to evolve systems called MNCGs (Metal Nanocluster Composite Glasses) characterized by non linear optical features. For the final properties of MNCGs, shape and dimensional

distribution of nanoparticles are fundamental and therefore a synthesis route that allows a deep control of these parameters is needed. The general approach to realize MNCGs is to use a synthesis made by two steps at least: the first step is the introduction of a dopant species inside the glassy matrix, the second step is a treatment of the doped glass by energetic techniques with the aim of inducing the clusterization of the dopant ions; in this frame ion exchange is one of the most used ways of realizing the glass doping [1].
Copper shows features similar to those of silver and for that reason it has been widely studied too. The peculiarity of copper is that it possesses three oxidation states (metallic state, 1+ and 2+) related with each other by a dismutation equilibrium that in glass makes the control of the oxidation state ratio complicated.

1.2.1 The ion exchange techniques

During the ion exchange the matrix is placed directly in contact with a source of the doping element. In that condition, a concentration gradient between the substrate surfaces and the dopant source is developed and the diffusive migration of the dopant inside the matrix occurs. Three different experimental setup are possible to be used and in general they are classified as follow: thermal ion exchange, field-assisted ion exchange and the field-assisted solid state ion exchange (FASSIE).
Hereinafter a brief description of the ion exchange techniques is reported.

1.2.2 Thermal ion exchange

The pure thermal ion exchange is realized when the tank of the foreign element is a fused salt containing the dopant ions and the glass is dipped inside the bath for a specific period of time; this is the easiest setup to realize the IE and it is also known with the name of ion exchange by molten bath. The diffusion phenomenon obtained is a thermal activated process generated by the concentration gradient between the molten salt bath and the glass and it could be controlled by changing the experimental parameters: bath temperature, glass composition, time of exchange, bath composition. The temperature must be controlled and maintained lower than the T_g of the

glass to avoid the softening of the matrix. About the choose of the bath, nitrate salts are the most used due to the low melting points of this class of compounds but also mixture of different salts at the eutectic point were used to lowering the needed process temperature [23].
The figure 1.1 schematically shows the exchange process during the immersion of glass into the fused salt. The mobile ions (usually monovalent ions such as Na^+ in the case of silicate glasses) diffuse outward the glass and they are replaced by the inner diffusion of dopant ions from the salt bath toward the glass surfaces; the diffusion takes place on all the glass surfaces directly in contact with the fused bath.

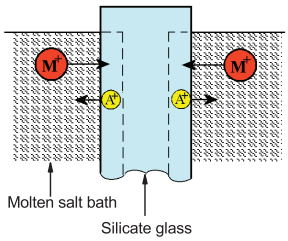

Figure 1.1: Representation of thermal ion exchange process.

1.2.3 Field-assisted ion exchange

The ion exchange by fused salt does not have high diffusion rate when it is applied to multivalent ions with low diffusivity. In that case, an external electric field can be applied to the fused salt to promote the diffusion obtaining the so called field-assisted ion exchange [24]. In general the applied potential interacts with the multivalent ions inducing an electric force that drives the diffusion of the ions. That is also true for the monovalent mobile ions of the glass, that diffuse deeply inside the matrix. The field-assisted ion exchange can be thought as a thermal activated process driven by the concentration gradient and by the electric field and it is represented in figure 1.2. The diffusion by field-assisted ion exchange can be controlled acting on all over the setup parameters mentioned before for thermal ion exchange and on the characteristic of the electric field too.

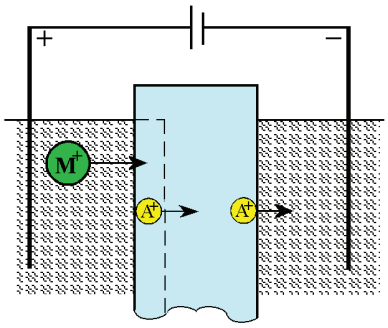

Figure 1.2: Representation of field-assisted ion exchange process.

1.2.4 Field-assisted solid state ion exchange

The last typology of setup for the ion exchange is the field-assisted solid state ion exchange (FASSIE), where the source of the dopant element is a metallic film deposited over the glass surface via sputtering or by thermal evaporation of a metallic target. The glass with the deposited metallic film is closed between two metallic plates acting as electrodes and placed inside a oven at temperature not higher than the T_g; applying a potential between the two electrodes, the oxidation of metallic film is induced at the interface between the deposited film and glass surface due to diffusion of negative oxygen ions coming from the glass itself: then under the effect of the electric field the positive ions start to diffuse into the glass [25]. Also in this case there is not the retro diffusion of the monovalent ions from the matrix but their migration toward the deepest layer of the matrix. This particular experimental setup can be an alternative when the melting point of the salt required is higher than the T_g or if the salt fumes are toxic. The process is shown in figure 1.3.

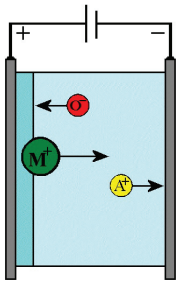

Figure 1.3: Representation of the field-assisted solid state ion exchange process.

1.2.5 The exchange apparatus

The ion exchange processes realized for the synthesis of the samples reported in this work have been done by the use of an electric oven; the possible working range temperature is between RT and 1200 °C and the temperature control is about 5 °C around the set point. The furnace has room of about 1700 cm^3 inside that the melting pot with the salt mixture is placed. This setup has been expressly upgraded with an electric engine (5-6 Hz) for the sample rotation. This solution has been adopted with the aim of homogenizing the fused salt during the exchange by a stirring action, to obtain more homogeneous samples. The specimen is linked to the electric engine with a steel stick. 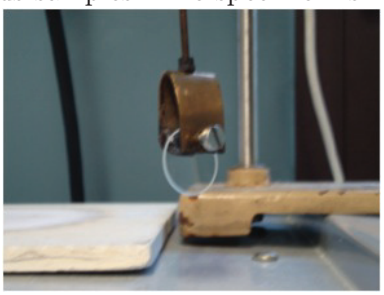

CHAPTER 2

Characterization techniques

2.1 Optical Absorption (OA)

When the light interacts with the matter it can be diffused, transmitted or absorbed. The absorption of light occurs when impinging photons have energy comparable to the energy gap between two electronic states of the absorbing system. When this condition is satisfied, an effective probability exist for the photon to be absorbed by the molecule. The technique based over the selective absorption of light by a medium is known as *optical absorption* (OA) and it can be used to study gaseous, liquid or solid samples. The analysis is made changing the wavelength of an incoming light source of intensity I_0 and measuring the intensity of light transmitted I across the sample of thickness x, being these two quantity analytically related by the Lambert Beer's law (2.1):

$$I(x) = I_0 \exp(-\alpha x) \tag{2.1}$$

where α is a constant value called absorption coefficient.
When solid samples are analyzed by optical absorption, the interaction of light with matter has an absorption and a scattering aspect too. These two contributions are introduced in equation 2.1 with the *extinction coefficient* β (2.2). In the expression of β, N is the number of absorbing (or scattering)

species, V is the sample volume and σ_{ext} is the *extinction cross section* where the probabilities for a photon to be absorbed (σ_{abs}) or scattered (σ_{sca}) are contemplated inside (2.3).

$$\beta = \frac{N}{V}\sigma_{ext} \tag{2.2}$$

$$\sigma_{ext} = \sigma_{abs} + \sigma_{sca} \tag{2.3}$$

Using β the equation 2.1 becomes

$$I(x) = I_0 \exp(-\beta x) \tag{2.4}$$

from that it is possible to define the *optical density* (O.D.) as:

$$O.D. = \log\left(\frac{I_0}{I}\right) = [\log(e)]\beta x \qquad . \tag{2.5}$$

Optical density expresses the damping of the light across the sample and the spectrum recorded is called *extinction spectrum*.
The OA is a useful techniques for studying glasses doped with transition metal. Generally speaking, when glasses doped with transition metals are analyzed by OA the extinction spectra could show bands due to the inter-band transition of the doping atoms, allowing to obtain information about the oxidation state. Furthermore, another type of signals could be present if metallic nanoparticles are buried inside a dielectric host. When the imping-ing light hits the nanoparticles, the electromagnetic radiation interacts which nanoparticles and generates a collective oscillation of the electron clouds in resonance with the forcing electric field, as described in Chapter 5. That os-cillation is called surface plasmon resonance (SPR) and generates a signal in the extinction spectra. The position of SPR mainly depends on the chemical element and on the matrix whereas the shape and the intensity are affected by the dimension, shape and number of the particles too.

2.2 Photoluminescence

The absorption of energy by a system induces a transition from the ground state (gs) to an excited state (es) of the electrons. When the system relaxes towards the gs the most common via for loosing its exceeding energy is

the emission of light. The features of the emitted light are related to the characteristics of the system and for that it can be used to study the system. On this phenomenon several analytic techniques are founded and the term luminescence indicates the ensembles of techniques where the light emission is not induced by heat absorption. More deeply, when the energy source consists on photons the technique associated is called *photoluminescence* and for definition, it indicates the light emission typically in UV-VIS or infrared wavelength range stimulated by the light absorption. The general processes of energy absorption and release of energy are resumed in figure 2.1.

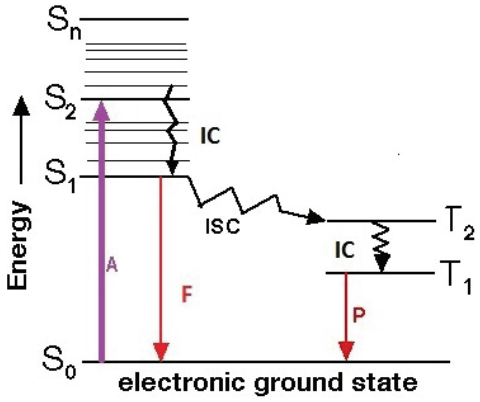

Figure 2.1: Representation of photoluminescence process where: A = photon absorption; F=fluorescence; P=phosporescence; S=singlet state; T=triplet state; IC=internal conversion (non-radiative transition); ISC=intersystem crossing.

After the photon absorption two different transitions are possible for the system relaxation: the non-radiative and the radiative. The non-radiative transition (indicated as internal conversion) does not generate light because the exceeding energy is lost by vibrational, rotational and translational mechanisms and thus heat is produced; non-radiative transition can occur only if the neighboring of the excited species are able to absorb heat. In the second type of transition, the radiative one, the system relaxes toward the gs by means of light emission. Two different types of radiative transition exist: the *fluorescence* and the *phosphorescence* transition. Fluorescence occurs when two states of singlet ($S_1 \rightarrow S_0$) are involved during the transition from

the es to the gs. On the contrary, if the relaxation changes the molteplicity state of the system (the transition arises from a triplet excited state to a singlet ground state $T_1 \rightarrow S_0$) the phenomenon is called phosphorescence. The singlet state is more energetic than the triplet state and it possesses a life time of 10^{-11} s $\div$ 10^{-9} s shorter than the triplet life time (10^{1} s $\div$ 10^{-3} s) and as a consequence of that the fluorescence emissions occur much faster, on the order of 10^{-8} s.
The photoluminescence study is realized by an spectrofluorometer apparatus with that three different kind of analysis can be done. In the first the sample is irradiated by a fixed wavelength and the light emitted inside a specific wavelength range is recorded. The result is called *emission spectrum* and often it is indicated as PL. The second mode of analysis consists on changing the excitation wavelength and recording the intensity at only one emitted wavelength usually taken out from the PL analysis. This is similar to an absorption spectrum and it is in general indicated as *excitation spectrum* (PLE). The last typology of analysis consists on the measurement of the luminescent decay duration called *life-time measurement*. In this measurement the samples is irradiated with a pulsed light source of the right wavelength to stimulate a precise luminescent emission; the pulse duration must be shorter than the emission life-time to avoid interference by the light source.

The photoluminescence analyses presented in this work have been collected at the Optic Laboratory of Veneto Nanotech S.C.p.A. (Porto Marghera-VE-Italy) by a modular setup Fluorolog 3-21TR320-TCSPC-NIR (Jobin Yvon) equipped with Xe lamp (450 W) as light source.

2.3 Rutherford Backscattering Spectrometry (RBS)

Rutherford Backscattering Spectrometry (RBS) is a nuclear non-destructive analysis technique which lets one to obtain information about the qualitative and quantitative composition of thin samples without using standards. In this technique an accelerated beam of light ions (usually helium ions or protons) is directed on the sample usually placed in a vacuum room (figure 2.2). The analysis consists on the determination of the energy of the light ions backscattered by the sample atoms (E_1) and on their count. Assuming

only elastic collisions, knowing the initial energy of the accelerated beam (E_0) it is possible to obtain information about the composition of a sample, being E_0 and E_1 linked each other by the equation 2.6

$$E_1 = KE_0. \tag{2.6}$$

K is the *kinematic factor* and depends on the scattering geometry (angle θ), the mass of the impinging ions (m_p) and the target atoms mass (m_t) (equation 2.7)

$$K = \left[\frac{m_p \cos\theta + \sqrt{m_t^2 + m_p^2 \sin^2\theta}}{m_p + m_t}\right]^2. \tag{2.7}$$

The number Y of deflected ions with a certain outgoing energy (E_{out}) collected inside a solid angle (Ω) under the detector is expressed by the equation 2.8 where σ is the differential scattering cross section: the backscattering yield is linked to the surface density (Nt, where N is the sample density and t is the analyzed thickness) of the scattering ions inside the sample

$$Y(E_{out}, \theta) = \frac{d\sigma(E_{in}, \theta)}{d\Omega}\Omega(Nt)\frac{Q}{q_{ion}}. \tag{2.8}$$

When the collision between the target atoms and the probe nuclei occurs under the surface layer the energy measured is affected by an energy loss contribution due to the interaction of probe with the electronic clouds of the sample atoms. Usually these events have a high probability to occur so the energy loss can be considered as a continuous process along the incoming and outgoing path. Taking into account the energy loss due to the backscattering events inside the sample, the outgoing energy is expressed by equation 2.9 from that is possible to extract information about the concentration in depth

$$E_{out}(t) = K(E_{in} - \Delta E_{in}) - \Delta E_{out}. \tag{2.9}$$

Is worth noting that RBS does not give chemical information (oxidation state, chemical bonding ...); light elements (atomic weight comparable with the probe's one) are not easily detectable and overlap between signals can occur. At last it is usually possible to get information only about the first 1-2 μm in depth.

RBS analysis has been done at IFNM National Laboratories of Legnaro (PD-Italy) with a 2 MeV $^4He^{2+}$ ions beam under a backscattering angle of 160°.

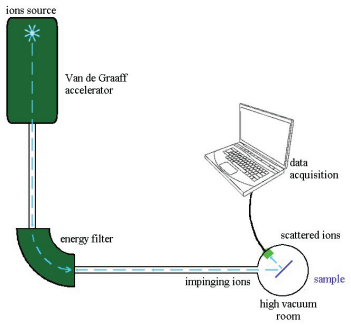

Figure 2.2: Layout of RBS apparatus.

2.4 Solar simulator apparatus and the solar cell test

A solar simulator is an apparatus that allows to measure the power produced by a PV panel when it is irradiated with an artificial light source like a lamp; the spectrum of wavelengths emitted by the lamp must be similar to the sun spectrum as much as possible.
The typical analysis made by a solar cell simulator consists on the measurement of the current produced as a function of the cell potential (I-V); from that it is possible to extract the output power produced (equation 2.10)

$$P = V * I \tag{2.10}$$

where: P is the power [W]; V is the potential [V]; I the current [A].
Moreover form the I-V analysis it is possible to extract the cell characteristic parameters: the short circuit current, the open circuit voltage, the maximum power produced and the filling factor. The open circuit voltage (V_{OC}) is the maximum voltage available for a PV cell and it is defined as the voltage at current equal to zero. Differently, the current measured when the applied bias at the cell is zero (short circuit condition) is called current of short circuit (I_{SC}) and it stands for the highest current produced by the cell. The

I-V sweep lets us to measure the output current by PV cell between I_{SC} and V_{OC} and then to calculate the power produced (for additional explanation, see Appendix A). Taking into account the definition of power, at I_{SC} and at V_{OC} the power is zero but the product between these two quantities is the power produced by the cell if that one works ideally. Considering all those parameters it is possible to define the filling factor (FF) as ratio between the real maximum power output by the cell and the theoretical power of cell (2.11):

$$FF = \frac{V_{MP} * I_{MP}}{V_{OC} * I_{SC}} \tag{2.11}$$

where V_{MP} and I_{MP} stand for the voltage and current at the point of max power measured by the system. So it is easy to understand the FF is an evaluation of solar cell quality.

To analyze the down-shifting systems studied in this thesis a home-made solar simulator apparatus was evolved. That system is composed by a DC power supply, a light source, a solar panel and a digital multimeter (Tektronix KEITHLEY 2410). The DC supply is directly linked to the lamp and the multimeter is connected to the cell; the light is hold on the top of an iron structure and the cell is perpendicular placed under the light source on the plane below. The solar cell used in this apparatus is a commercial device made of four PV elements inside; being the dimension of the cell much bigger than the exchanged area of the samples it has been needed to extract a photovoltaic element of comparable dimension with the glass and to cover the exceeding area by a dark mask. The setup was equipped by a 12 V halogen lamp (Osram) as light source; this lamp is generally sold for civil application and, as outcome of safety laws, halogen lamps are closed with an UV filter. In fact it is well known halogen lamps emit along all the visible range in a continuous way until the near UV range and, being UV light potentially dangerous for the human wellness, they must be avoided (the producer declares a transmission percentage close to zero for wavelength shorter than 350 nm). The UV-filter could be a constrictive condition for the testing of down-shifting systems and so with the aim of improving the lamp emission under 350 nm the UV filter was removed.
Using this apparatus the first measurements realized were the I-V sweeps of

the bare solar cell; this kind of study is useful for our purpose because it lets us to understand the properties of the cell used and for the comparison of the data collected. The figure 2.3 shows the I-V sweep of the bare cell; in this picture the value of I_{SC} an V_{OC} are indicated too. Applying the equation 2.11 the filling factor parameter has been calculated and it resulted to be 0.7. In the same picture also the outputted power produced by bare PV cell evaluated applying the relation 2.10 is plotted.

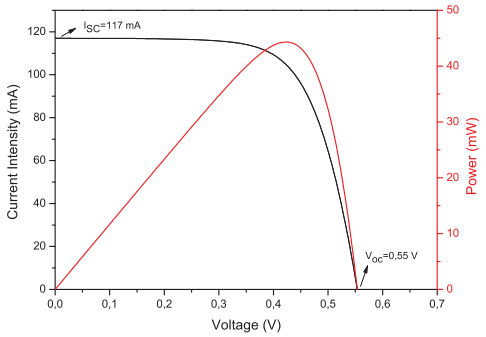

Figure 2.3: I-V sweep of the bare solar cell.

The I-V sweep of uncovered cell has been collected for thirty five minutes by steps of 5 minutes and the results are reported (figure 2.4 and 2.5). During the observation period I_{SC} is not constant, it decreases for the first 20 minutes and then random oscillation are recorded; as consequence the power produced by the PV panel changes with time too. In general an alteration on I_{SC} value is due to a non homogeneous light source and so what appears from this first analysis is that the setup is not able to provide stabilized and constant condition for the measurement of the cell yield. That is due to the fact the light source is not commensurate for that kind of applications and the system is heavily affected by the environment. Nevertheless on the basis of these results a specific measurement protocol was evolved to analyze the samples under the best conditions. Every measurement session starts after 5 minutes of PV cell irradiation under the lamp; the determination of I_{SC} and V_{OC} were done after 5 minutes of irradiation and after 20 seconds of recording. Before and after the analysis of a sample, the I-V sweep of the cell cover by the undoped glasses is recorded.
The figure 2.6 compares the behavior of the cell with and without the cover glass before the ion exchange. When the cell is covered the outputted power decreases due to the intrinsic optical features of the glass, mainly the ab-

sorption and the reflection of light.

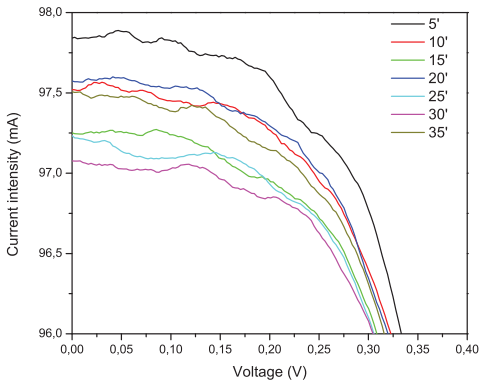

Figure 2.4: I-V sweeps collected from the bare solar cell.

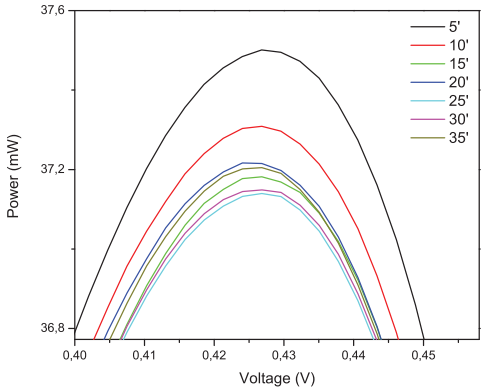

Figure 2.5: Power produced by the bare solar cell.

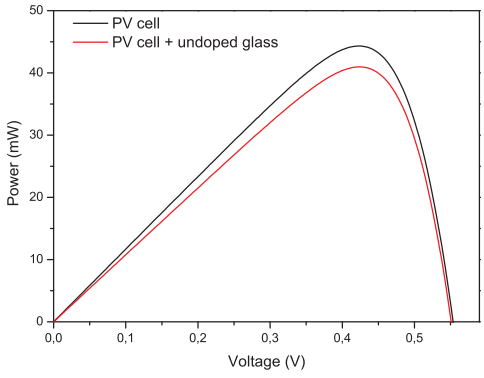

Figure 2.6: Comparison between the power produced by the bare solar cell (black) and the power outputted from solar cell covered by the undoped glass (red).

2.5 X-ray Absorption Spectroscopy (XAS)

X-ray Absorption Spectroscopy (XAS) is a type of absorption spectroscopy based on the Lambert Beer's law where the electromagnetic probe is a beam of X-photons of energy usually between 10 to 10^3 keV. This technique is able to give information about both the geometric and electronic local structure of matter. XAS experiments are usually performed by using synchrotron radiation sources, for their intense and easily tunable X-ray beams. Samples can be in the gas-phase, solution, or condensed matter (i.e. as solids). When X-ray radiation goes through a solid sample, its intensity decreases mainly by three different phenomena: the photoelectric absorption, the scattering of X-photons due to light-matter interaction, and the creation of a electron-positron pairs as a consequence of the interaction between the X-photon and the electrostatic field surrounding a charged particle. In the typical energy range used for XAS (10 to 10^3 keV), photoelectric absorption is the most important because the X-photon scattering has a low probability to occur and the electron-positron creation is prohibited (figure 2.7).

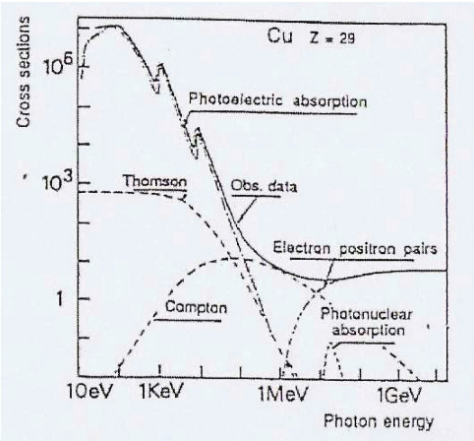

Figure 2.7: X-ray absorption cross section for copper.

Photoelectric absorption phenomena occur when X-photons have an energy equal to a threshold value determined by the needed energy for an electronic transition to some unoccupied state. The energy threshold depends on the electronic energy levels of the atoms in the investigated system: for a given electronic transition, it increases with the atomic number Z and it is specific for each atomic species (figure 2.8).

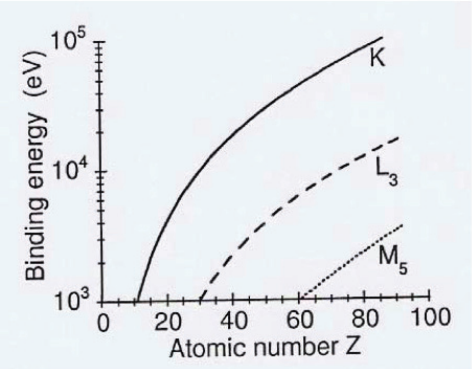

Figure 2.8: Binding energy of some core levels.

In the condensed matter, at energies lower than a given absorption threshold the absorption coefficient shows a slow decreasing value by increasing the X-ray energy; when the threshold energy value is reached, a strong increase of the absorption coefficient is detected. By further increasing the X-ray energy, oscillations of the absorption coefficient are recorded and a fine structure is generated in the spectrum (figure 2.9). By the study of the fine structure features it is possible to find out information about the absorbing species and about their surrounding environment. The spectrum obtained by the XAS data can be divided into two energy regions: the X-ray Absorption Near Edge Structure (XANES) and the Extended X-ray Absorption Fine Structure (EXAFS) ones. XANES is related to the fine structure shown about 150 eV over a given absorption threshold. In this energy range the photoelectron has a wavelength similar to the interatomic distances, whereas its mean free path is larger. By the study of XANES fine structure one can obtain information about the local electronic structure, the configuration of the ligands and some information of the emitting atom oxidation state. The fine structure located from XANES region up to 1000 eV over the absorption edge falls in the so-called EXAFS energy region. Here the photoelectrons are characterized by wavelengths lower than the interatomic distances and by mean free paths close to tens of Angstrom. From EXAFS measurement, one can get information about the average interatomic distances, coordination numbers, thermal and structural disorder.

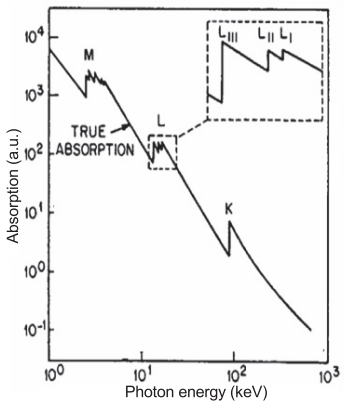

Figure 2.9: Absorption coefficient behavior respect to the energy of the X-ray photons.

XAS analysis can be realized through two different approaches:

- transmission mode: in this case the intensity (I_0) of the impinging X-ray beam on the sample and the transmitted intensity (I) are measured;
- fluorescence mode: the absorption coefficient is obtained by the measurement of the photons emitted by fluorescence as a consequence of the X-ray photoelectric absorption. In this case, the number of photons with an energy related to a specific relaxation transition for the absorbing atomic species is evaluated. The fluorescence mode approach is mandatory when: a) the sample absorption is so low that the transmitted X-ray beam has not detectable intensity decrease if compared to the incoming one; b) the sample absorption is so high to prevent the detection of the transmitted X-ray beam.

XAS measurements reported in this thesis were performed at XAFS beamline of ELETTRA synchrotron facility in Basovizza (Trieste, Italy); the storage ring operated at 2.0 GeV in top-up mode with a current of 300 mA. Spectra were collected at room temperature in fluorescence mode at Cu K-edge (8979 eV).

CHAPTER 3

The optical basicity effect on silver oxidation state

In the previously chapter, speaking about the ion exchange techniques, it has been reported that one of the parameters to control the process is the glass composition. In fact, it is well known the oxidation state of a dopant atom as a TM inside a glass is dependent on the interaction between dopant and matrix too. The first attempt to express this relation has been the Lux-Flood theory that depicts the acid-base characteristic of an oxidic medium by the oxide ion activity; this approach has shown some limitations and only restricted validity [26] [27] [28]. Successively a second approach based on the application of Lewis's acid-base theory was proposed. In this frame the oxidic medium acts as an electron density donation center (Lewis's base) and the metal acts as an electron density acceptor (Lewis's acid) [29]. The degree of that behavior is expressed by the optical basicity (OB, Λ) that nowadays is a formal way to express the relationship between the guest redox ratio and the host. Optical basicity expresses the willingness of oxygen atoms of a silicate medium to donate negative charge and it could be thought as a measurement of the electron density inside a cationic site. The general accepted definition for optical basicity is: the electron donation power of the oxygen ions or atoms compared to the one of crystalline CaO (the optical basicity of crystalline CaO is conventionally defined as equal to the unity) [30]. The determination of the donation power can be made by the UV spectroscopy techniques, taking advantage of the Nephelauxetic effect. The Nephelauxetic

effect is a well know phenomenon of the inorganic chemistry and it is related to the energy shift of a transition metal complex molecular orbital due to the ligand field generated by ligands. The first effect related to that is the shifting of the guest absorption bands. In the case of an oxidic medium, the optical basicity can be measured from the red shift induced by the donor power of the environment on the absorption bands of a probe element introduced inside the matrix. Tl^{+}, Pb^{2+} and Bi^{3+} (external configurations $6s^2$) were the most typical probe elements used because their 6 s−6p transition undergoes to a red shift from UV to visible wavelengths with the increasing of donor power of the matrix [29]. On this base the optical basicity is defined as (3.1):

$$\Lambda = \frac{\nu_f - \nu}{\nu_f - \nu_{\mathrm{CaO}}}. \tag{3.1}$$

In equation 3.1, ν_f is the absorption frequency of probe element as free ion (gaseous state), ν is the measured absorption frequency and ν_{CaO} is the frequency of the probe ion absorption band measured inside crystalline CaO [30]. The measurement of OB from refraction index evaluations was proposed too but this approach has been shown to be feasible only if the cations have a low refractivity or otherwise if the cations are not concentrated and the system does not undergo to important structural changes [31].
The spectroscopic measurements have shown the possibility to calculate the OB of an oxidic medium directly from its composition by means of the basicity moderating parameter, γ, expressing the attenuating influence of every elements on the oxide ions donation power [30]. For example, in the case of an oxidic medium composed by two different oxidic components A and B (oxidation state a^{+} and b^{+} respectively) in the proportion of x:y, the Λ can be calculated by (3.2) [29]

$$\Lambda = X_A \frac{1}{\gamma_A} + X_B \frac{1}{\gamma_B} \tag{3.2}$$

where X is the equivalent fraction (3.3)

$$X_A = \frac{ax}{ax + by}; \tag{3.3}$$

the table 3.1 resumes the moderating parameters of some elements expressed as oxides. For a single oxide component the equation 3.2 becomes

$$\Lambda_i = \frac{1}{\gamma_i} \tag{3.4}$$

so the equation 3.2 can be rewritten as (3.5) [29]:

$$\Lambda = X_A \Lambda[oxide(A)] + X_B \Lambda[oxide(B)] + ... \tag{3.5}$$

The equation 3.5 is additive for every oxide components and it can be adapted in a similar way to calculate the optical basicity of multicomponent oxidic systems [30].

Element	γ	Λ
Cesium(I)	0.60	1.7
Potassium(I)	0.73	1.4
Sodium(I)	0.87	1.15
Lithium(I)	1.0	1.0
Barium(II)	0.87	1.15
Strontium(II)	0.91	1.1
Calcium(II)	1.00	1.00
Iron(II)	1.0	1.0
Manganese(II)	1.0	1.0
Magnesium(II)	1.3	0.78
Aluminium(III)	1.65	0.60
Silicon(IV)	2.1	0.48
Boron(III)	2.36	0.42
Hydrogen(I)	2.5	0.40
Phosporus(V)	3.0	0.33
Sulfur(VI)	4.0	0.25

Table 3.1: Values of γ and Λ for some elements expressed as oxides. [29]

The optical basicity is a significant parameter into different areas and it has been successfully applied in relation to the glass matrices but also into the steel industry, mineralogy and ceramic area [32] [33] [34].
The study of the relation between the optical basicity of a matrix and the

oxidation state of a TM has been widely studied up to now. What has been well established is that the chemical state is shifted towards the highest oxidation state if the optical basicity is increased; that is true for all the TMs studied. A particular case is represented by copper for that the redox state decreases with the increment of the optical basicity [35] [36]. The results presented in this thesis will be discussed on the base of these evidences.

3.1 Objective of this work

The first aim of this work is to study the relation between optical basicity and the oxidation state of a transition metal at temperature below transition temperature T_g. The interest towards this study is inherent to the hypothesis that the optical basicity can be a fundamental parameter for the study of the silicate glasses doped by ion exchange.
In the introduction of this manuscript it has been reported the ion exchange is a technique widely used for the glass doping. Up to now a lot of work about the influences of the matrix characteristic, expressed by the optical basicity degree, on the TM oxidation state has been done but the biggest part of these studies are related to TMs doped glasses produced by melt quenching technique (for example see [37]). Being ion exchange completely different from the melt quenching process it is important to verify how the optical basicity of a glass interacts with the oxidation state of a dopant in case of ion exchange process; that could be important to better understand how to control the chemical state of a TM and then the final optical properties showed by the doped glass. To do that three glasses with different optical basicity were doped by ion exchange with silver and then analyzed by spectroscopic techniques. Silver has been chosen for doping the glasses because of its high diffusion coefficient in silicate glasses, thus allowing an easy and effective doping of the glass surface. Furthermore silver has only two oxidation state: 1+ and the metallic one. For all of that silver represents a preferred choice.
The study presented hereinafter would be a first step in that direction. In my knowledge only Svecova et al. [38] and Capek et al. [39] have done a similar study before now.

3.2 Experimental

Soda-lime glass (SL), BK7 Schott borosilicate glass (BK7) and a UV400 clear Corning glass were doped with silver by thermal ion exchange process using the exchange apparatus described inside subsection 1.2.5. The glasses were dipped in $AgNO_3$:$NaNO_3$ 1% mol. salt bath at the temperature of 400 °C for 60 minutes under stirring condition (5-6 rpm). After the exchange the samples were analyzed by optical absorption, RBS and photoluminescence spectroscopy. The composition of the different type of glasses is reported in table 3.2; for each glass the optical basicity degree was calculated by eq. 3.5.

Component	**Soda-lime**	**BK7**	**Corning**
O	59.6	60.2	60.6
Si	23.9	22.4	16.5
Na	10.2	3.8	2.0
Ca	2.4	traces	traces
K	0.5	1.8	2.3
Mg	2.6	/	traces
Al	0.8	/	3.6
B	/	11.0	11.2
Ti	traces	/	traces
Ba	/	0.8	0.7
Zn	/	traces	/
Pb	/	traces	/
Zr	/	/	0.6
Sr	/	/	traces
Sn	/	/	0.1
Cu	/	/	0.1
Li	/	/	2.3
Fe	/	/	traces
Optical Basicity	**0.58**	**0.53**	**0.51**

Table 3.2: Composition of the glasses studied in this work reported as atomic percentage.

3.3 Results and discussion

3.3.1 Rutherford backscattering spectrometry

An example of the recorded RBS profile is shown in figure 3.1 where the principal element edges are evidenced.

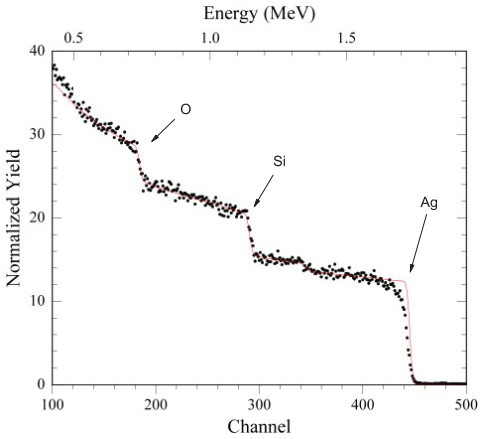

Figure 3.1: RBS profile of Λ=0.58 glass after the ion exchange process. In red, spectrum simulation.

From the simulation of the profile it has been possible to obtain an evaluation of the dopant atoms concentration and some characteristics of the exchange dynamic.

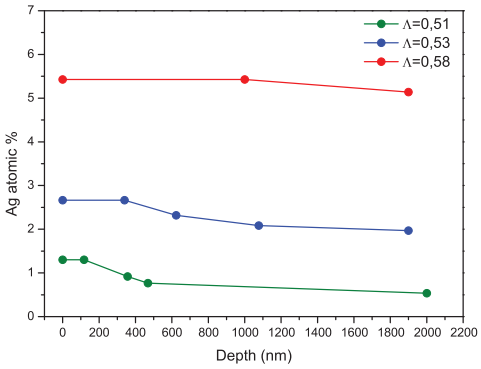

Figure 3.2: Silver ions diffusion profile inside the different glasses as obtained by RBS. The relative uncertainty on the concentration values is of the 10 %.

As can be seen from figure 3.2 the glass with highest OB degree results the heaviest silver doped one with a silver surface concentration of 5.5%

and almost constant over the entire analyzed thickness. For this sample the diffusion process involves sodium and potassium ions too in accordance with:

$$2\,Ag^{+}_{bath} \leftrightarrows 1\,K^{+}_{glass} + 1\,Na^{+}_{glass}.$$

For every two silver ions migrating inside the matrix a sodium and a potassium ion migrate outward the matrix making available some structural sites for the silver diffusion. The glasses with OB equal to 0.53 and 0.51 have a concentration of silver at the surface around 2.5% and 1.3% respectively; under the surfaces the dopant concentration gradually decreases. Differently from the soda-lime glass (Λ=0.58) the exchange seems to be compatible with a one to one process between the silver and the potassium ions

$$1\,Ag^{+}_{bath} \leftrightarrows 1\,K^{+}_{glass}.$$

The differences on silver surface concentration measured are mainly due to the differences on alkali composition of the three glasses but it is important to underline these are not related to the donor power features of the matrix (optical basicity). In the introduction chapter, describing the ion exchange process, it has been outlined how the dopant concentration is related to the lattice sites made available by the diffusion out of the glass of mobile species, such as sodium and potassium ions; as a consequence, it is possible to assume that the higher is the alkali concentration the more will be the number of dopant ions diffusing inside glass. Comparing the alkali composition of the three matrices with the silver surface concentration, table 3.3 clearly shows the decrement of the concentration is linked to the initial alkali concentration in the matrix.

Glass	Λ	Na%	K%	Ag%
Soda-lime	0.58	10.2	0.5	5.5
BK7	0.53	3.8	1.8	2.5
Corning	0.51	2.0	2.3	1.3

Table 3.3: Comparison between alkali composition of glasses and surface silver concentration.

In case of BK7 glass (Λ=0.53) and Corning glass (Λ=0.51), the final dopant concentration is affected not only by the alkali concentration but also by the

exchanging species. RBS simulations showed for Λ=0.53 and 0.51 glass the exchange was realized manly with potassium even if, considering their ions dimension, potassium is expected to have a diffusion coefficient lower than sodium (K ionic radius =1.38 Å, Na ionic radius =1.02 Å). Here, the mixed-alkali effect probably comes into play to affect the final diffusion coefficients ([2] and refs therein). Moreover, the presence of boron can obstacle the diffusion because, being boron part of the glass network, it makes the matrix closer and more rigid. As a consequence, in BK7 and Corning glass the diffusion of silver ions results hindered and the surface final concentration lower than for soda-lime glass.

3.3.2 Optical absorption

The figure 3.3 reports the optical absorption spectra of the undoped glasses studied in this chapter.

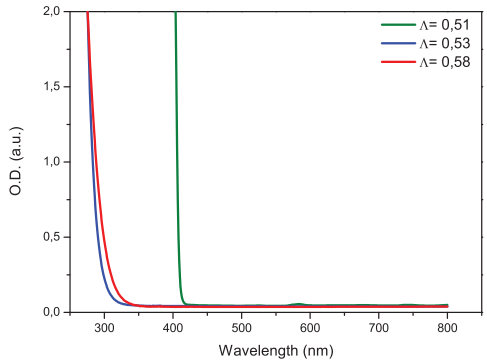

Figure 3.3: Optical absorption spectra of undoped glasses.

The glasses with Λ of 0.58 and 0.53 (soda-lime and BK7 respectively) show the typical "near-UV" absorption cut-off at 300 nm due to the alkaline ions in the matrix. Corning glass spectrum (Λ =0.51) shows an absorption edge at about 400 nm due to differences in glass compositions. This matrix is composed by elements as Cu, Sn, Sr, Ti, Fe not present inside SL and BK7 glass and characterized by absorption bands under 400 nm [40].
After the exchange the increasing of optical density are observed due to the presence of dopant atoms inside the glass (figure 3.4).

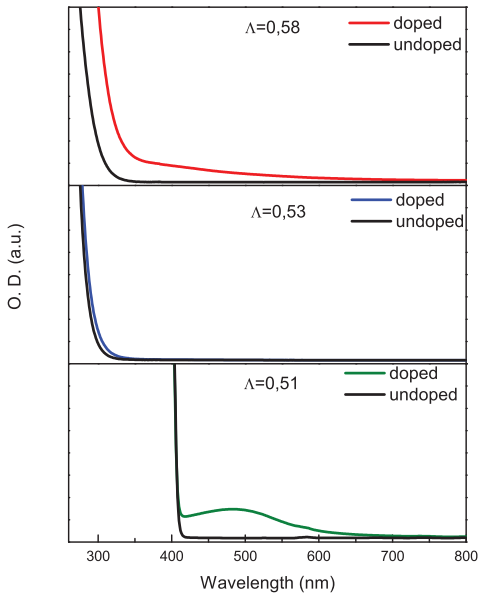

Figure 3.4: Optical absorption spectra of glasses after ion exchange.

The optical absorption spectrum of Λ=0.53 glass shows a weak increasing of optical density around 300 nm generated by the intraband transition of Ag^+ ions [41]. For Λ=0.58 the already noticed silver ions band at 300 nm increases in intensity but a tail of absorption is clearly noticeable over 350 nm; this last one has been associated to silver multimeric complexes [42]. Focusing on the lowest optical basicity glass (Λ=0.51) no absorption signals due to Ag^+ ions and silver complexes are evident, being probably covered by the glass cut-off at 400 nm; despite that a new band centered around 500 nm is present. This bump could be related to the surface plasma resonance phenomena (SPR) indicating the formation of nanoparticles buried in glass. As reported previously (subsection 2.1) the SPR band position on spectrum is typical of the element constituent the cluster and of the dielectric matrix; for example in silica and many silicate glasses the silver SPR is located around 420 nm and the copper SPR is placed around 580 nm [43] [44]. In the case of silver doped Corning glass the band is located between the silver and copper SPR typical wavelengths making the assignment of the observed band not easy. One could assume that SPR at 500 nm is generated by silver-copper core shell structures or by Ag−Cu alloy nanoparticles. When core shell nanoparticles are embedded in glass the absorption spectrum shows the copper SPR separated from the silver SPR [45]. Differently silver-copper

alloy nanoparticles generate a SPR placed between 410 nm (Ag SPR) and 580 nm (Cu SPR) and the features of the SPR band change in function of the Ag/Cu ratio [46] [47] [48] [49]. Taking in account all these evidences, the position of the SPR signal recorded for Λ=0.51 glass is compatible with the formation of some kind of Ag-Cu alloy nanoparticles. Moreover from theoretical simulation of SPR profile by using the Mie's scattering theory it has been found that a refractive index increasing of the medium surrounding the particles can generate a red shift of the SPR band [50] [51] [52]. Considering then the broadness of the SPR band probably the nanoparticles are very small and then the alloying of silver atoms and copper could not be the only reason for the shifting of the SPR but also the glass index could give a contribute. It is worth to underline the supposed presence of nanoparticles alloy is a specific feature of this type of Corning glass due to its particular composition. A deep structural characterization is needed to prove the existence of silver-copper alloy nanoparticles. Another possible explanation is the formation of oxidic silver species that represent an intermediary step for the formation of silver nanoparticles [53].

3.3.3 Photoluminescence

Silver doped glasses are known to show different emission bands between UV and visible wavelength range. When Ag-doped silicate glasses are irradiated by near UV light, a band between 300 nm and 350 nm and an emission around 450 nm (blue emission) are expected to be found. Moreover an orange emission (600 nm) is found when the doped glass is stimulated by a blue radiation. These features have already been studied by several groups during the years. The ultraviolet emission around 300 nm is associated to the $4d^{10} \rightarrow 4d^9\ 5s^1$ transition of Ag^+ ions as isolated emitter [54]. Differently the band around 450 nm (blue band) were found by Borsella et al. [55] inside high silver doped glasses and it was related to structure like $Ag^+ - Ag^+$ pairs [56]. The last emission expected, the orange one, is generally ascribed to the formation of silver multimeric complexes as $(Ag_2)^+$, $(Ag_2)^{2+}$, $(Ag_3)^+$ and $(Ag_3)^{2+}$; usually the position, the shape and the intensity of orange band are dependent by the "complex" ionization state [57] [58].
The figure 3.5 reports the luminescence features of the undoped glasses under an excitation wavelength of 260 nm; the sharp peak close to $2\lambda_{exc.}$ (512 nm)

on the emission spectra is an unfiltered spurious signal due to the Xe lamp. The glass Λ=0.58 and 0.53 show quite similar emission profile. The Λ=0.51 glass shows an intense emission around 450 nm; considering the composition of this glass it is possible to associate that signal to Cu^{+} ions in glass [59]. Increasing the excitation wavelength at 350 nm only the Λ=0.51 spectrum shows a weak but broad emission over 500 nm (figure 3.6).

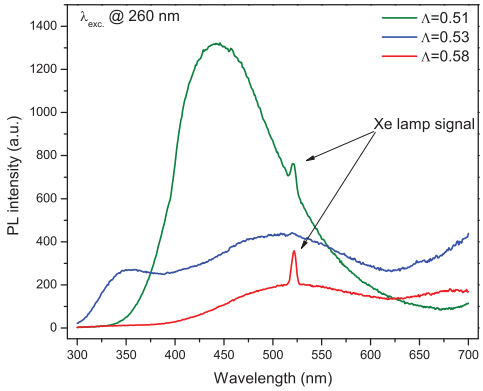

Figure 3.5: Photoluminescence spectra of undoped glasses; $\lambda_{exc.}$= 260 nm.

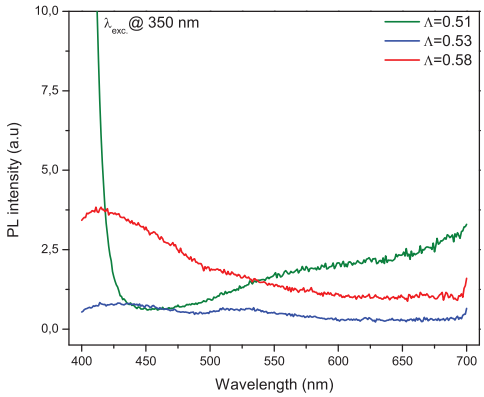

Figure 3.6: Photoluminescence spectra of undoped glasses; $\lambda_{exc.}$= 350 nm.

The analyses of the doped glasses are resumed in figure 3.7 (excitation wavelength = 260 nm). After the ion exchange all samples emit around 480 nm; this emission is the aforementioned blue band generated by the $Ag^{+}-Ag^{+}$ pairs. The band intensity increases from Λ=0.51 to 0.53 and then falls down for the most basic glass indicating the $Ag^{+}-Ag^{+}$ pairs are less present despite the high silver concentration.

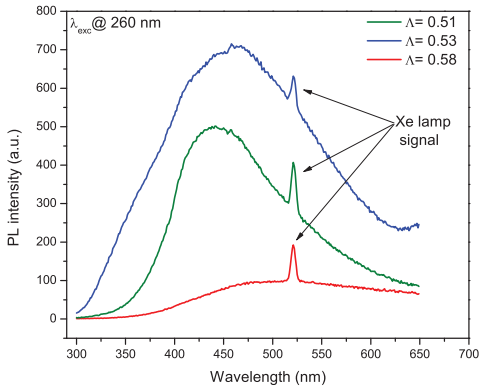

Figure 3.7: Photoluminescence spectra of doped glasses; $\lambda_{exc.}$= 260 nm.

The excitation spectra recorded at the wavelength near the maximum of the luminescent band (figures 3.8, 3.9 and 3.10) show an absorption profile between 300 nm and 350 nm due to the silver ions absorption. A particular case is the Corning glass (OB= 0.51) because for this samples the PL spectrum shows only the intensity diminution of the band initially associated to Cu^{+} ions but the shape and the position of this band appear unchanged. Moreover the PLE spectrum of the doped glass does not show any absorption increment amenable to silver ions.

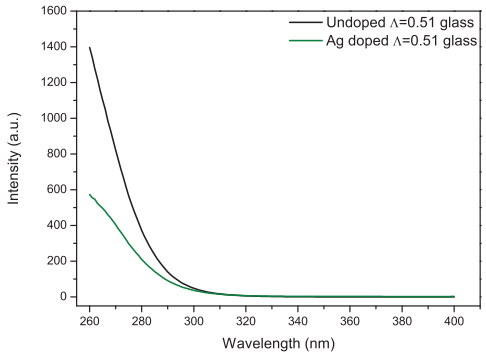

Figure 3.8: Excitation spectra of Λ=0.51 ($\lambda_{emis.}$= 480 nm, blue band).

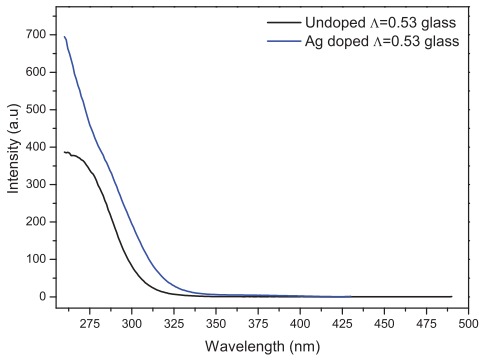

Figure 3.9: Excitation spectra of Λ=0.53 ($\lambda_{emis.}$= 480 nm, blue band).

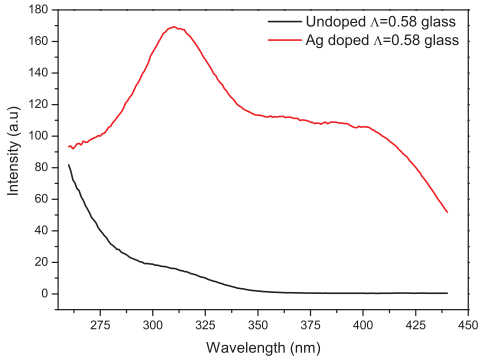

Figure 3.10: Excitation spectra of Λ=0.58 ($\lambda_{emis.}$= 480 nm, blue band)

Emission spectra were recorded using an excitation wavelength of 350 nm too. The results are reported in figure 3.11 and as it can be seen only the glass with Λ=0.58 shows a huge band over 600 nm; this emission is the typical orange emission generated by silver multimeric complexes.

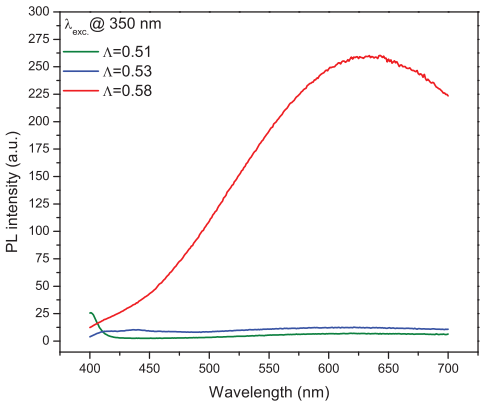

Figure 3.11: Photoluminescence spectra of undoped glasses; $\lambda_{exc.}$= 350 nm.

The related absorption band is located over 350 nm on excitation spectra (figures 3.12, 3.13 and 3.14). Increasing the optical basicity the absorption band is red shifted indicating that the absorbing species becomes more complex and less similar to a free silver ions. The biggest absorption was found for the Λ=0.58 due to the high concentration of silver complexes. This absorption signal is not present for the matrix with Λ=0.51 probably due to the absence of silver complexes.

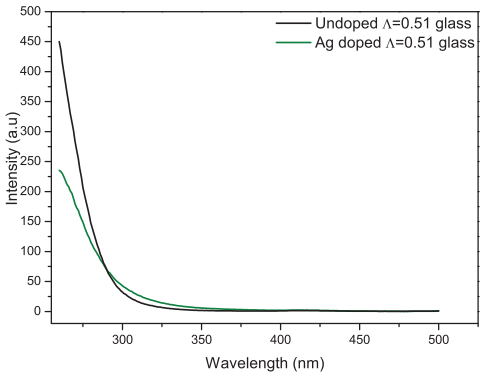

Figure 3.12: Excitation spectra of Λ=0.51 ($\lambda_{emis.}$= 630 nm, orange band).

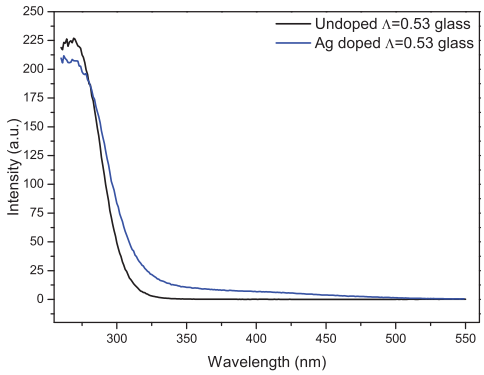

Figure 3.13: Excitation spectra of Λ=0.53 ($\lambda_{emis.}$= 630 nm, orange band).

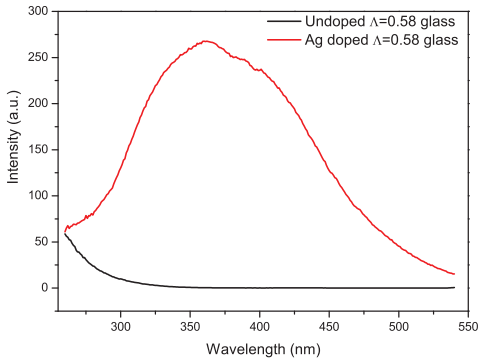

Figure 3.14: Excitation spectra of Λ=0.58 ($\lambda_{emis.}$= 630 nm, orange band).

3.4 Discussion

Three different types of glasses were doped with silver by pure thermal ion exchange process under the same synthesis condition. What clearly appears from the whole optical characterization is the progressive stabilization of Ag^{+} ions and multivalent silver structures as the optical basicity of glass increases; the term multivalent silver structure it is used to indicate silver aggregates of few atoms with cumulative positive charge at least 1+. This evidence is somehow in agreement with was already found at temperature well above T_g [35]. An interpretation of these results can be done by taking into account the oxygen chemical state expressed by the electronic polarizability α: the polarizability can be considered as the volume occupied by the electronic cloud of an atom or ion [60] or as the capability of the electronic cloud to be distorted by an electric field [61]. These two complementary works

depict how the power of donation of oxygen is affected by positive cations with different electronegativity as neighbors. Inside an oxidic medium the electronic cloud of oxygen will be somewhat distorted being the oxygen linked to other atoms like silicon, boron, aluminium ecc. When the optical basicity of the silica glass is increased by adding alkali metal ions (Na and/or Ca and/or K) the electronegativity of these elements can balance the electron clouds around oxygen with the result of changing the oxygen donor power. As a consequence, when a host ion as a transition metal is placed inside this system it can experience a more or less useful negative environment for the stabilization of its positive charge, depending on the matrix optical basicity degree [60]. It is important to underline that the cation stabilization is realized by the sharing of negative cloud from oxygen toward the TM ion and not through a true electron transfer [62]. Decreasing the capability of oxygen to share its negative cloud (a decreasing of its polarizability), the dopant ions become less stabilized and other processes can happen if there are the right conditions, like for instance the reduction of TM ions to the metallic state and the formation of nanocluster; the presence of SPR band on optical absorption spectrum of glass with Λ=0.51 confirms that hypothesis. Furthermore the orange band intensity close to zero shows the intrinsic glass features are not able to stabilize efficiently multivalent structures.

There is another important question to discuss; the possible formation of nanoclusters inside the glass with the lowest optical basicity degree. The formation of cluster is due to the reduction of silver ions to the metallic state and the growth of nanoparticles on the crystallization seeds [63]. Is not aim of this work to discuss the nucleation and growth of nanoclusters but some consideration on the reduction process of silver ions can be done. The formation of TM nanoparticles in glass is one of most controversial and open question of that research field. In general the interpretation of the formation of silver nanoparticles in glasses is done by two different approaches: the first assumes that the matrix defects are the electrons source for silver reduction [64], the second considers the presence of a real redox couple between silver and other elements with different potentials [65] [66].

Defects in a glass matrix are not to be thought as the alteration of an order (like for a crystalline structure) but for instance the lacking of bonds and then the presence of positive holes, negative charges and radical species. These defects have been widely studied in silica before and after γ-irradiation [67],

X-ray irradiation [68] or laser annealing [69] and some computational studies were done [70]. The same kind of defects were founded and studied in alkali silicate glasses [71] [72], phosphate glass [73] and borate glass too [74]. The most used technique for the defect analysis is the UV spectroscopy and being most of them paramagnetic center ESR (Electron Spin Resonance) is widely used too [75]. By using the notation proposed by David L. Griscom et al. [75] where $\equiv$ denotes three Si$-$O in the network and $\cdot$ an unpaired electron, the main defects in glasses and the position of the relative UV absorption band are listed in the following table 3.4.

Defect	**Structure**	λ **(nm)**
E'	$\equiv$Si$\cdot$	215, 239
POR	$\equiv$Si$-$O$-$O$\cdot$	239
NBOHCs	$\equiv$Si$-$O$\cdot$	405, 610
TE		305

Table 3.4: Structural defects in silicate glasses where POR means *peroxy radicals*, NBOHCs means *non bridiging oxigen hole centers* and TE means *trapped electron* [75].

Furthermore $\mu-$Raman spectroscopy can be used to study the role of matrix on the TM reduction following the evolution of Raman Q-band [76]. Related to that, an exhaustive collection of the Raman signals associated to the structural fragments was done by Matson et al. [77] and by McMillan [78]. The figure 3.15 reports the magnification of optical absorption analysis under 300 nm of Λ=0.51 glass. Before and after the ion exchange the spectra show detector saturation signals due to the high absorption of glass in the region under 400 nm. As a consequence of that, it is not possible to observe anyone of the fingerprint signals of matrix defects summarized in table 3.4 and for that reason it is not feasible to make experience of the eventually structural evolution of glass. At this point the role of the electrons pulled out from the glass matrix toward the silver redox equilibrium stays unknown but at first glance it can not be excluded without more specific analyses.

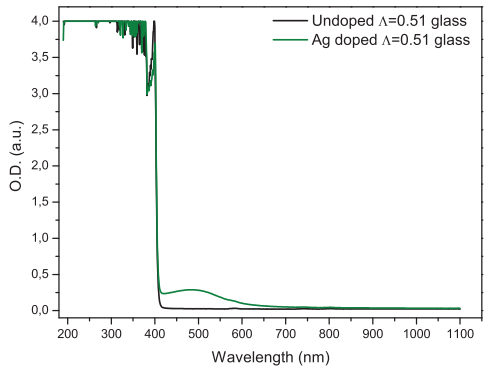

Figure 3.15: Magnification of optical absorption spectra relative to Λ=0.51 glass.

The redox equilibrium for a multivalent element in an oxide medium is express by

$$4M^{n+}_{(melt)} + 2mO^{2-}_{(melt)} \leftrightarrows 4M^{(n-m)+}_{(melt)} + mO_{2(gas)} \tag{3.6}$$

where: n indicates the oxidation state, M the multivalent element and m the number of electrons involved in the reduction. This equation resumes the parameters giving a contribute to the redox state control: temperature, oxygen fugacity, concentration of the multivalent ion [79]. Thinking to the possibility of a redox equilibrium in the glass, the easiest approach is to take into account the series of standard potentials. The series of standard potentials is referred to water as solvent and standard conditions (25 °C and 1 atm) so the information that can be figure out is in principle only qualitative. To inspect the presence of a redox equilibrium between the different elements inside the glass one should have a potential series referred to silica as solvent. That has already been investigated up to now and the most general approach has been to study the redox state after the quenching of a fused silicate glass containing the multivalent ions. For example Schreiber et al. studied the electromotive force series in a silicate fused glass and they evidenced how the temperature influences only on the absolute value of the element potential but it does not influence the series order [80]. Furthermore, in a borosilicate melt the absolute value of potential is affected by the glass composition and the only parameter that seems to affect the order of the potentials inside the series is the oxygen fugacity [79]. Redox potentials were measured for different ions in borosilicate glass and soda-lime glass by employing square-

wave-voltammetry too [81]. Considering that the glass with lowest optical basicity degree is a borosilicate one, the most useful potentials series is that proposed by Schrieber et al. [82], whose values for the transition metals present inside the matrix are resumed in table 3.5.

Redox Couple	**Potential** [V]
Ag^{+}/Ag^{0}	0.5
Cu^{2+}/Cu^{+}	-0.8
Fe^{3+}/Fe^{2+}	-1.7
Cu^{+}/Cu^{0}	-3.3
Ti^{4+}/Ti^{3+}	-5.0
Sn^{4+}/Sn^{2+}	-5.5
Fe^{2+}/Fe^{0}	-6.3

Table 3.5: Redox potentials for TMs present inside Λ=0.51 glass taken out from [82].

At the beginning the glass does not contain silver; from the series reported the most noble element is the copper because it shows the less negative potential and so it is reasonable to assume copper at the 1+ oxidation state. For example the following reaction could be proposed:

$$Fe^{2+} + Cu^{2+} \rightarrow Fe^{3+} + Cu^{+}. \tag{3.7}$$

After ion exchange process silver ions are introduced inside the matrix and, as is reported before (table 3.5), silver shows a redox potential higher than copper so a new reaction could be proposed:

$$Ag^{+} + Cu^{+} \rightarrow Ag^{0} + Cu^{2+}. \tag{3.8}$$

An additional proof of the reaction 3.8 can be found on luminescent properties of Λ=0.51. They could be interpreted as follows: the band at 450 nm of the unexchanged glass is the due to the luminescent features of the Cu^{+} ions. When silver ions are placed inside the matrix the reaction 3.8 occurs, copper ions oxidizes itself and reduce silver ions. As a consequence

the concentration of Cu^{+} decreases, so does the intensity of the band at 450 nm.

At last it is worth to underline the formation of clusters during the ion exchange process (SPR band in the optical absorption spectrum of OB=0.51 glass) is slightly unusual because the formation of metal cluster is in general observed after a post ion exchange energy treatment, such as thermal treatment [83], laser irradiation [84] or ion irradiation [85]. These treatments give energy to the doped glass, inducing phenomena (reduction, nucleation and growth) that bring to the clusters formation. Cattaruzza et al. [86] studied the MNCGs formation in silver doped soda-lime glasses by ion exchange; they obtained the raising of SPR band only after a thermal treatment in air at 500 °C or after a laser irradiation. In silver doped soda-lime glass Simo et al. observed an absorption band increasing around 400 nm after a thermal annealing at 400 °C: this absorption has been clearly assigned to SPR signal only after a treatment at 550 °C [53]. Formation of cluster at temperature below 500 °C can be justified as the consequence of the low optical basicity (less stabilization of the higher oxidation state) and by the considerable presence of reducing species. In fact, inside Corning glass reducing species are present in high concentration respect to the other glasses. As a consequence, the redox reaction between silver and other less noble metals results to be important and the formation of the first metal cluster seeds can occur without inducing their formation by a post doping treatment.

3.5 Conclusions

In this work glasses with OB of 0.51, 0.53 and 0.58 have been doped with silver by ion exchange and characterized by nuclear (RBS) and optical techniques (optical absorption and fluorescence spectroscopy) that allowed us to obtain information about the concentration and oxidation state of the dopant. In the case of soda-lime glass (OB=0.58) the huge orange emission (PL analysis) and the absorption increasing over 350 nm on optical absorption spectra have been interpreted as the consequence of the multivalent silver structures formation. The optical absorption spectrum collected in case of Λ=0.51 (glass with the lowest optical basicty) showed the SPR signal, evidencing the probable formation of nanoparticles during the exchange process. On the basis of the SPR position one could assume the formation silver-copper alloy nanoparticles but further structural analyses are needed to verify that; for example high-resolution TEM could be an useful tool to study the shape, the dimension and the composition of the nanoparticles. Finally, the silver reduction to the metallic state has been justified on the basis of a redox reaction between silver and copper but, by taking advantage of EPR and μ-Raman analyses it will be possible to obtain information about the matrix contribution to the reduction process of the dopant.
Concluding, the main information obtained from this study is that the highest oxidation state of TM ions is progressively stabilized inside matrices of high optical basicity degree also if the TM is introduced inside hosting medium by ion exchange. This results is in agreement with the general knowledge about the relation between the OB and TM oxidation state of doped glasses produced by melt quenching technique. A possible development of this work could be the systematic study of the TM oxidation state (for example silver) referred to wide range of optical basicity degree. To do that it is important to have the possibility of change the glass composition. This could be possible for instance by taking advantage of the sol-gel approach to realize glass layers of different composition (and then OB) inside that to study the chemical state of silver placed by ion exchange technique. Moreover it will be important to deal with the study of the more complex case of copper oxidation state.

CHAPTER 4

Luminescent down-shifting panels for photovoltaic cells

The idea of producing current from light was proposed by Edmond Becquerel during the first half of the nineteenth century and from that the interest has grown from laboratory scale until the industrial scale. The first type of solar cell widely diffused on the world trade, known as the "first solar cell generation", were based on the crystalline silicon (c-Si) or multy-crystalline silicon (mc-Si). With the improvement of technology and of the industrial processes a second generation of photovoltaic (PV) panels was evolved thanks to the thin films technology used to create new types of active medium. In particular this new class of active mediums are based on the amorphous silicon (a-Si), polymeric films coupled with semiconductor junctions [87] or inorganic based films as cadmium indium selenide (CIS) [88] [89], copper indium gallium selenide (CIGS-cell) [90] [91] and gallium arsenide (GaAs) [92] [93]. The most negative feature of the solar technology is the inability of taking advantage from all the sunlight spectrum for the current production; in fact the spectral conversion of solar cell expressed as external quantum efficiency (EQE) falls down in the region of blue-UV radiation principally due to additional losses at the top of the panel introduced by the industrial production [94]. Moreover the PV panels evolved up to now present other types of spectral loss sources as for instance the part of incoming sunlight not absorbed because the photon energy is lower that the band gap of semiconductor, the thermal losses due the absorption of too energetic incoming photons [94],

the recombination phenomena near the surface that reduces the absorption of high energy photon [95]. As a consequence, the efficiency of the solar cell is not so high as it could be expected. For example, the theoretical efficiency for a c-Si solar cell was calculated to be around the 31% [94] [96] but the real terrestrial modules efficiency are close to the 22% for the first generation module based on c-Si and between 10% and 15% for the second generation panels; an exception is represented by AsGa thin films whose efficiency reach the 23.5% [97]. Being the low efficiency the major drawback of the solar technology evolved up to now, the research is working to improve this limit and in particular it is looking on the enhancement of shorter wavelength absorption [94]. For reaching this goal two different approaches are actually explored. The first approach is to evolve new kind of systems with the peculiarity to use in a better way all the incoming sunlight radiation. This new class of PV panels represents the so-called third generation and it is composed by multjunction [98] [99], heterojunction [100] and intermediate band gap cells [101] [102]. Moreover, the last frontiers of the solar cell evolution is the study of quantum dots [103] and nanoporous or nanocomposite materials [104] [105] [106].
The second approach studied is to evolve additional systems that allow the solar cell to take advantage of the shortest wavelength radiation. In general these systems are layers showing particular optical features as down-conversion or down-shifting phenomena. Being these systems directly applied onto the solar cell they represent a passive approach because the solar cell properties are not changed.

4.1 The down-shifting frame

The down-shifting is a type of passive approach based on the most elementary fluorescent process to improve the photovoltaic yield; the first examples of down-shifting were proposed in the seventies by A. Goetzberger et al. [107] and by Hovel et al. [108]. The down-shifting is generally realized by putting between the cover glass and the solar cell a layer that contains a luminescent system. The luminescent species absorbs radiation at wavelengths mainly at the edge between UV and VIS wavelength range and then emits photons at longer wavelength inside the spectral region for that the solar cell shows the highest properties of spectral conversion. Due to the presence of the down-

shifting layer the number of photons reaching the solar cell is increased, the number of charge carriers became greater and the spectral conversion too (EQE is increased). Referring to the typical solar cell parameters (FF, I_{SC}, and V_{OC}) it is important to note the first effect of down-shifting process is to increase only I_{SC} of the cell but the V_{OC} and the FF are unchanged. Nowadays the research are oriented on the evolution of new passive LDS (luminescent down-shift) materials but to be successfully applied on the field of LDS some fundamental properties are needed to be fulfilled. The host medium should possess these features [94]:

- high transmittance all over the wavelength range of maximum spectral conversion for the cell;
- photostability (the performance must remain over 80% of the initial along 20-25 years);
- they must be optimum environment for the hosting of the luminescent species;
- not to be altered by the manufacturing process.

Differently luminescence elements must have the following characteristics [94]:

- wide absorption band in the wavelength region of the lowest cell EQE;
- narrow emission band inside the region of the highest cell EQE;
- highest separation between absorption and emission band (no overlap);
- high absorption coefficient;
- luminescence quantum efficiency (LQE) close to the unity;
- photostability over 20-25 year at least.

In general the light absorption by the host, the luminescence quantum efficiency below the unity and the overlap between absorption and emission bands represent the main limitations to the gain introduced by the LDS. Furthermore, the presence of an additional layer inside the photovoltaic panel can introduce other loss sources due to reflection of light between interfaces and lateral losses too. At last it is important to take in account the economic

aspect too; LDS materials must be as cheap as possible to make convenient the production on a large scale.
Up to now various types of host have been studied and they range from the organic matrix like poly-vinil-acetate (PVA) [109] or poly-metil-metacrylate (PMMA) [110] [111] to the inorganic ones as CaF_2 or Al_2O_3 [108] [112]. About the luminescence species, the most widely investigated as possible candidate are: quantum dots (QDs), rare earth ions (RE) and organic dyes (ODs).
Semiconductor quantum dots (QDs) possess very interesting luminescence features. The QDs show high luminescence efficiency and tuneable optical properties [113]: in fact, absorption features are related to the dimension of the QDs and the size distribution affects the Stokes' shift [114]. Some examples of QDs performances applied as down-shifting luminescent materials can be done: silicon quantum dots hosted in glass and applied over c-Si solar cells improve the cell efficiency of about 0.4% [115]; conversely, if the QDs are hosted in SiO_2 the solar yield seems not to increase [116]. CdSe QDs rise up the efficiency of a mc-Si solar device between 6.3% and 28.6% as a function of the illuminating spectrum [117].
RE element ions are studied in the field of LDS for their high luminescence quantum efficiency; however, their main drawback is the low absorption coefficients [114]. Total absorption can be raised by increasing the RE layer thickness and/or the RE ions concentration, on the meantime avoiding clustering effects that heavily decrease the energy transfer phenomena and the luminescent efficiency [118]. Furthermore, the luminescent emission can be enhanced using an organic ligand acting as sensitizer or antenna for the RE emitting species [113]; as a consequence, these systems are usually know as rare-earth organic complexes or organolanthanide complexes. Due to the organic ligand acting as sensitizer, these systems show large Stokes' shifts and self-absorption phenomena are completely avoided [119] [120] [121]. Experimentally, the RE-LDS materials efficiency varies with the solar cell used; nevertheless, the Si-based cells result to be the most sensitive to the presence of a RE-LDS layer [114]. Europium seems to be the most interesting luminescent RE in the down-shifting frame; for example Eu^{3+} ions hosted in PVA layer onto a c-Si solar device generate a performance difference of 2.8% [122] and of 9.5% if RE ions are placed in SiO_2 [123]. The gain of 5% was measured by using Sm^{3+} ions in $KMgF_3$ host on a CdS/CdTe solar cell [124].

Eu^{3+} phenantroline in ORMOSIL (organic modified silica host) changes the c-Si performance of the 18% [125]. About the a-Si solar cell, Eu^{2+} ions in CaF_2 resulted in a performance difference of 50% [126] and Tb^{3+} bypyridine in ORMOSIL host increases the performance by 18% [125].
Organic luminescent dyes have been studied for the spectral conversion too. As shown by Richards et al. ODs are very useful to increase the solar cell efficiency mainly at low wavelengths. ODs can be used alone or blended with other ODs to enlarge the range of wavelengths absorbed [111]. Examples of gain obtained using ODs in PMMA host are: rhodamine 6G (c-Si) 48% [127], rhodamine 6G (GaAs cell) 3% [108], coumarine 540 (GaAs cell) 3% [108], lumogen-F (violet570 + yellow083) (mc-Si) 0.3% [128], coumarine (polymer solar cell) 0.7% [129] and lumogen-F (CdS/CdTe cell) 17% [111].
The study of LDS systems concerns also the valuation of the obtained gain by the application of a LDS over a solar cell; in literature the theoretical calculation and/or the experimental gain estimation is often presented. Klampaftis et al. in their review pointed out the problem of the solar cell yield testing. They compared the results obtained by testing a multi-crystalline silicon cell (mc-Si) covered by a PMMA layer doped with the optimum dye mix, using different spectra for illumination of the solar device (the same was done using a CdTe solar cell instead of mc-Si). The most important result is the evidence that gain changes as a function of the incident spectrum [94]. Despite PV community has established the standard method for the test is to use a AM1.5G spectrum lamp [130] of 1 sun intensity ($1000W/m^2$), in literature this protocol is often not followed and a wide variety of spectra is used for yield measurements. As a consequence, comparison among LDS systems is complicated and it should be made with caution due to the large disparity of the test condition employed [94]. Moreover, Klampaftis et al. outlined the different observed results are due to the large variety of systems studied and on the procedure used for the test too, for instance the solar cell used and the comparison of the behaviour with the uncoated cell one, or the presence of the anti-reflective coating (ARC) on the solar device. In general the efficiency of a LDS results to be dependent on the solar cell where it is applied and, in particular, to the EQE at low wavelengths of the solar device.
About the use of silver or copper ions inside the cover glass panels for down-shifting application, Zakhidov et al. observed a gain of 1.6% when silver inside phosphate glass is used as LDS [131]. An example of copper ions glass

for down-shifting can be found in the work proposed by Gómez et al. but they did not report a measurement of the gain obtained by this kind of LDS [132].

4.2 The main objective

The aim of this work is to study the possibility to realize down-shifting phenomena directly inside the solar cell cover glass panels by doping them by ion exchange. Putting the luminescent element inside the cover glass, it will be possible in principle to avoid the limits due to the introduction of a supplementary layer over the cell because no additional lateral losses are introduced; furthermore, the glass is in principle a chemical and mechanical stable material, cheap and also it is a good environment for the dispersion of luminescent TMs. The choice of taking advantage from ion exchange process is another selling point because is a cheap, easy and widely studied technique. Being this study somehow oriented towards a possible industrial application of the doped glasses, it has been chosen to work on the glass type usually used for the photovoltaic panels. These panels are made of soda-lime glass (table 4.1) produced by float process (Pilkington S.p.A).

Component	**Atomic %**
O	60.3
Si	24.9
Na	8.9
Ca	3.3
Mg	2.2
Al	0.2
K	0.2
Zr	>0.01
Cl	>0.01
Ti	>0.01
Fe	>0.01
other elements	traces

Table 4.1: Pilkington glass composition.

4.3 The float glass

Nowadays the glass slides are produced mainly by float manufacturing process also known as Pilkington method. The innovative characteristics of this process is that it makes possible to obtain glass slides with virtually parallel surfaces and high optical features in a relatively easily way without mechanical processes. In this process, after the furnace, the fused glass passes continuously over a fused tin bath under controlled environment condition of temperature, atmospheric pressure and composition. The fused glass floats and spreads itself over the tin bath forming parallel and levelled surfaces; the glass side not directly in contact with tin bath are also fire polished. During the floating the diffusion of tin inside the glass occurs because it is favored by the high temperature and the concentration gradient realized between the tin bath and the glass. The resulting penetration of tin is determined by the manufacturing conditions in terms of temperature profile, impurity in the atmosphere and inside the tin bath, time of contact between glass and bath [133]. The tin contamination is not avoidable and it represents the major drawback of float process; for that reason float glass is studied to understand how the tin can affect the physical and structural properties of glass as well as how to control the tin diffusion for tailoring the final characteristics. For example Hayashi et al. [134] have observed the tin concentration is the main parameter affecting the mechanical properties. Moreover they have detected the role of tin on the ion exchange reactions at the basis of the weathering phenomena. Takeda [135] has investigated the tin effect on silver and oxygen diffusion inside float glass. He observed the diffusion rate is different for both glass sides and the oxygen diffusion is inhibited due to the reaction with the Sn ions. Moreover he collected the silver SPR signals only on the tin side of glass as the result of redox interaction of silver with tin. Zhang and coworkers [136] proposed a model to describe the tin diffusion with the aim of using it to control the real diffusion process during the floating. Dimitrova et al. [137] obtained the coloration of float glass with no need to any reducing agent. They exposed the glass at CuCl fumes and they observed the reduction of copper favored by the presence of tin. A similar study on the coloration of float glass doped by silver and copper was done by Dimitriev

et al. [138].

4.4 The choice of dopant species

The choice of the TM used for the glass doping by ion exchange was done following these criteria:

- luminescent properties compatible with the down-shifting process;
- diffusion properties;
- the glass after the doping should show high optical quality in terms of transparency and less coloration as possible.

On the basis of optical properties and of diffusion features both silver and copper could be good candidate and for that some preliminary ion exchange experiments were done. The silver optical features have already resumed on the chapter 3; the copper optical feature are resumed hereinafter.

4.5 The copper optical features

Copper in a glass matrix shows three different optical absorption bands in function of the redox state. In general, to Cu^{+} ions is associated a typical absorption signal placed around 280 nm [139] [140] while Cu^{2+} ions generate a broad absorption band spread between 790 nm and 810 nm [141] [142]. Differently if copper nanoclusters are embedded inside a glass a SPR band is expected around 560 nm [143].
The luminescence features of copper in glass are already known and a widely literature exists. When an UV light is used for excitation, cuprous ions exhibit a blue-green emission around 520 nm generated by the $3\,d^9 4\,s^1 \rightarrow 3\,d^{10}$ transition [144]. This band is influenced by the hosting matrix [145] and by the local atomic order [146]; in pure porous silica two bands at 430 nm and 490 nm are found from copper inside cubic site and octahedral distorted site respectively [147] [148]. Ti et al. [149], in relation to a strong emission around 510 nm, found a band between 260 nm and 310 nm on the excitation spectrum associated to the absorption of Cu^{+} ions inside an octahedral site tetragonal distorted. Fujimoto et al. [150] recorded an emission band around

550 nm that changes in shape and intensity if the excitation wavelength is changed between 270 nm and 350 nm; from the PLE analysis the absorption band due to Cu^{+} ions resulted centred around 260 nm and 290 nm. At last, when an excitation wavelength around 320 nn is used in presence of copper, an emission over 600 nm (orange-red emission) could be observed; this band has been associated to the formation of structures like $(Cu^{+})_2$ (copper pairs) and it was detected for copper ions in glass, crystalline $CuLaO_2$ and $CuZr(PO_4)_3$ too [59] [151] [152] (also demonstrated by computational calculation [153]).

4.6 Silver: first attempts

4.6.1 Experimental

To dope the PV glass panels, Ag^{+}-Na^{+} ion exchange has been realized by immersion of the matrix inside a fused $AgNO_3$:$NaNO_3$ (1:99) salt mixture. The exchange was performed at the temperature of 320 °C for 60 minutes following two different procedures: some samples were doped by immersion inside the fused salt (indicated as 'dipped') while other glass slices were doped floating on the bath surface, with the tin rich side not in contact with the bath. After the doping, some samples were annealed in air at the temperature of 350 °C for 1 h or 16 hours or at the temperature of 400 °C for 1 h.

4.6.2 Results

The optical absorption spectra of the samples exchanged by dipping or by floating are reported in figure 4.1. Considering the dipped samples, the as-exchanged glass shows a red-shift of the UV absorption edge generated by the intraband transition of silver ions. The same result was obtained for the as-exchanged sample prepared by floating, but in the case of dipped sample the edge shift is higher due to both the contribution of two surfaces to the total absorbance and the possible presence of small aggregates, like $(Ag_3)^{2+}$.

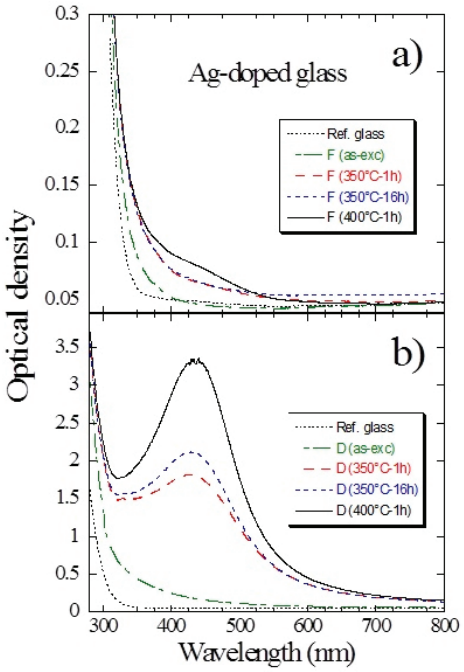

Figure 4.1: Optical absorption of cover glass doped by floating (panel **a**) or by dipping (panel**b**) in $AgNO_3$:$NaNO_3$ (1:99) salt bath, and subsequently thermal treated.

The spectra of the floating samples annealed at temperature lower than 400 °C show only the increment of the absorption over 350 nm associated to the silver complexes absorption. In case of the dipped samples, after the thermal treatment a well-defined band at 430 nm is present which can be attributed to the SPR of silver aggregates.
The optical absorption spectra of the samples showing the SPR band have been simulated by means of the Mie's model to get information about the mean size of the embedded silver nanoparticles. The Mie's model gives an analytic expression of the extinction cross section (σ_{ext}) to describe the optical response of composite systems form by metallic nanoclusters embedded in dielectric media. The theory has been evolved for diluted system (i.e., for metal filling factor $V_{cl} \ll 1$) and for spherical metal particles of radius R much lower than the incident light wavelength (usually few nm of size); the latter condition defines the so-called quasi-static regime. In this regime, the metallic nanoparticle experiences the electric field of the incoming electromagnetic wave as constant in space but variable in time; as a consequence, the interaction between light and particle induces a rigid oscillation of particle free

electrons with respect to the particle centre, thus originating an oscillating electric dipole (dipole approximation). Moreover in the quasi-static regime it is possible to neglect the effects related to the multipole momentum (for instance, magnetic dipole and electric quadrupole moments) simplifying the description. The expression for σ_{ext} in the Mie's theory is:

$$\sigma_{ext}(\omega) = 9\frac{\omega}{c}\epsilon_m^{3/2}V_{cl}\frac{\epsilon_2}{[\epsilon_1(\omega)+2\epsilon_m]^2+\epsilon_2(\omega)^2} \tag{4.1}$$

where V_{cl} is the filling factor (also called volume fraction) of the metallic nanoparticles, ϵ_m is the dielectric function of the host transparent medium (in this case ϵ_m is simply the square of the refractive index), $\epsilon_1(\omega)$ and $\epsilon_2(\omega)$ are the real and the imaginary part of the metallic nanoparticle dielectric function, respectively. The maximum value of the extinction cross section is attained when the denominator of equation 4.1 reaches its minimum value; in most cases it simply happens at the frequencies for which:

$$\epsilon_1(\omega) + 2\epsilon_m \cong 0 \tag{4.2}$$

and so when :

$$\epsilon_1(\omega) \cong -2\epsilon_m \tag{4.3}$$

The frequency that minimizes the denominator corresponds to the SPR band detected in metal nanocluster composite glasses. The real and imaginary part of the metallic nanoparticle dielectric function $\epsilon(\omega)$ in equation 4.1 can be obtained by the following relation 4.4, starting from the bulk metallic dielectric function: the dependence of the metallic dielectric function from the nanoparticle radius R is introduced to take into account quantum confinement phenomena in case of particle size less than the electron mean free path (i.e. usually less than 10 nm).

$$\begin{aligned}\epsilon(R,\omega) = \epsilon_{bulk}(\omega) + \omega_p^2\left(\frac{1}{\omega^2+\Gamma^2} - \frac{1}{\omega^2+\Gamma(R)^2}\right) + \\ + i\frac{\omega_p^2}{\omega}\left(\frac{\Gamma(R)}{\omega^2+\Gamma(R)^2} - \frac{\Gamma}{\omega^2+\Gamma^2}\right)\end{aligned} \tag{4.4}$$

where: ω_p the plasma frequency, Γ is the experimental damping constant of

the bulk metal and

$$\Gamma(R) = \Gamma + a\frac{v_f}{R} \tag{4.5}$$

(where a is a geometrical constant of value close to the unity and v_f is the Fermi velocity). The simulation of the experimental SPR bands has been done by using the expression proposed by Quinten for the bulk silver dielectric function [154]; we obtained a mean particle diameter of 1.6 nm, 1.8 nm, and 2.0 nm for the samples 350 °C-1 h, 350 °C-16 h, and 400 °C-1 h respectively.

Photoluminescence spectra were recorded by using an excitation wavelength of 260 nm (figure 4.2 a). As it can be seen, the spectra are characterized by the presence of the blue emission (420 nm) generated by silver pairs; this emission increases its intensity after thermal treatments. The same analyses, performed on the tin contaminated side of the dipped samples, did not show this feature, probably because the reduction of Ag^+ and the silver aggregation to form metal particles leave a very low amount of silver pairs inside the matrix.

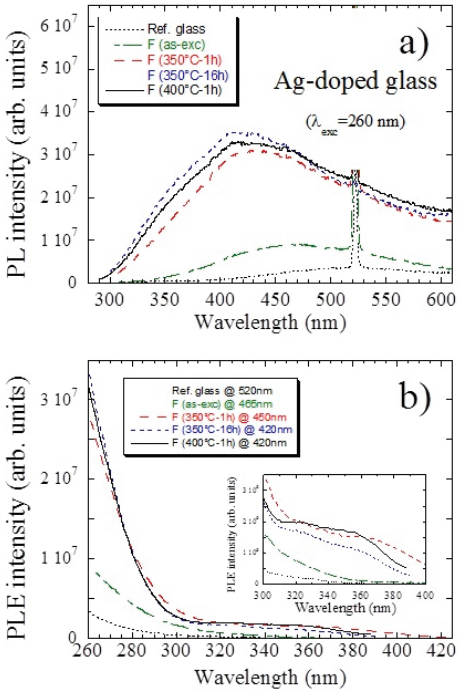

Figure 4.2: PL spectra (panel **a**, $\lambda_{exc.}$= 260 nm) and PLE spectra (panel **b**, $\lambda_{emis.}$= 430 nm) of cover glass doped by $AgNO_3$:$NaNO_3$ (1:99) salt bath. The sharp peak close to $2\lambda_{exc.}$ in the PL spectra is an unfiltered spurious signal due to the Xe lamp.

From the excitation spectra (figure 4.2b) it results that the blue band is excited mainly in the UV region and between 300 and 425 nm, showing a shift at higher wavelengths after thermal annealing. Increasing the excitation wavelength from 260 nm to 340 nm, the annealed samples exhibit the PL band around 600 nm (figure 4.3a); this band can be associated to the typical orange emission generated by the formation of silver complexes (like $(Ag_2)^+$, $(Ag_2)^{2+}$, $(Ag_3)^+$ and $(Ag_3)^{2+}$) .

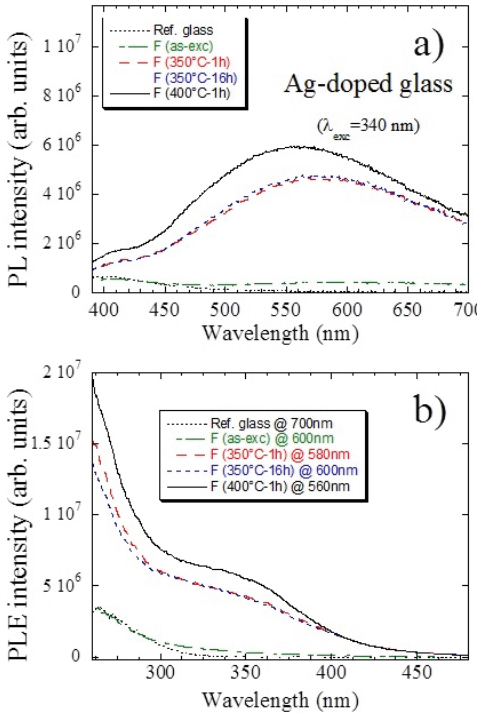

Figure 4.3: PL spectra (panel **a**, $\lambda_{exc.}$= 340 nm) and PLE spectra (panel **b**, $\lambda_{emis.}$= 550 nm) of cover glass doped by $AgNO_3$:$NaNO_3$ (1:99) salt bath.

This emission increases with the annealing temperature; in particular for the 350 °C samples the intensity does not depend on the annealing time, as previously observed for the pairs band, while it is higher for the sample treated at 400 °C for 1 h. The PLE related spectra (figure 4.3 b) show a broad and intense absorption band around 350 nm. These PLE and PL spectra outline how both the pair and the aggregate signals can absorb the light in the 300-400 nm wavelength range with a consequent emission in the visible range, which is quite interesting for the modification of the solar spectrum for commercial photovoltaic panels.

4.7 Copper: first attempts

4.7.1 Experimental

The copper doped PV panels were realized by using two different salt bath: a $CuSO_4$:Na_2SO_4 mixture at the eutectic composition (45:55) at the temperature of 550 °C for 20 min and a CuCl:$ZnCl_2$ mixture (11:89) at the

temperature of 350 °C or 400 °C for different times between 20 min and 16 h. For both the copper salts used the glasses were doped by totally immersion. After the exchange no systematic heat treatments in air were performed.

4.7.2 Results

After the doping by $CuSO_4$:Na_2SO_4 salt bath, the glass resulted transparent but colored by green and red. The optical absorption spectrum for this sample is proposed in figure 4.4; the absorption profile shows the copper nanoparticles SPR signal at 560 nm which lowers the glass transparency in the visible region, with a detrimental effect for solar applications. The well-defined absorption band around 700 nm could not be associated to the Cu^{2+} ions because in general cupric ions absorption originates a very broad band placed over 700 nm. The signal recorded under 700 nm could be ascribed to some multipolar effects as consequence of the dimension and/or a possible non-spherical shape of the copper nanoparticles: actually, a simulation (in the Mie frame, for spherical nanoparticles) of the SPR peak centred around 560 nm suggested a mean copper particle radius well over 10 nm.

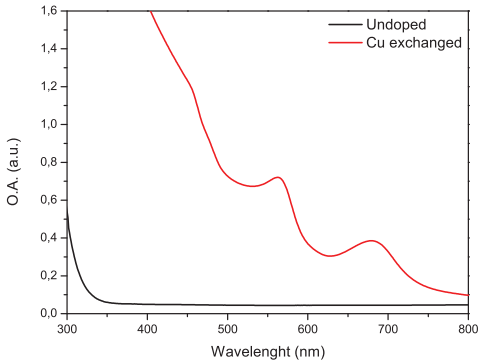

Figure 4.4: Optical absorption of cover glass doped by dipping in $CuSO_4$:Na_2SO_4 at the eutectic composition (45:55 % mol.) and at the temperature of 550°C for 20 minutes.

Due to the strong coloration and the high absorption feature of this sample, the $CuSO_4$:Na_2SO_4 bath has been discharged.
As reported on the experimental part PV glass panels were also doped by the CuCl:$ZnCl_2$ mixture. Nebolova et al. [155] have already studied this salt bath, obtaining a glass mainly doped by Cu^+ ions (the optical absorption

analysis showed only a red-shift of the glass edge). They justified this fact invoking the capability of Zn^{2+} of preventing the oxidation of cuprous ions. After immersion in CuCl:$ZnCl_2$ salt bath the Cu atomic percentage was measured by RBS. At the sample surface the copper is around 1 atomic % and after 20 min of ion exchange at 350 °C the Cu-doped region is extended over 2 μm in depth. Looking for the increasing of the dopant concentration, it has been chosen to realize exchanges at the temperature of 400 °C. Actually, from simulation of the RBS profile collected in the sample exchanged for 4 hours at 400 °C, the Cu depth profile resulted quite flat within the probed region, suggesting that the whole exchanged layer should be of some tens of microns. For the sample exchanged at 400 °C the RBS analysis was performed on different points of the surface too. By these studies it has been evidenced the surface accumulation of either Cu or Zn forming large opaque island on the glass surface as showed by the scanning electron microscopy analysis (most probably zinc chloride, as suggested by the energy-dispersion spectrometry analysis, EDS). The formation of 'salt islands' is generated by the interaction between the fused salt and the glass surface (figures 4.5 and 4.6).

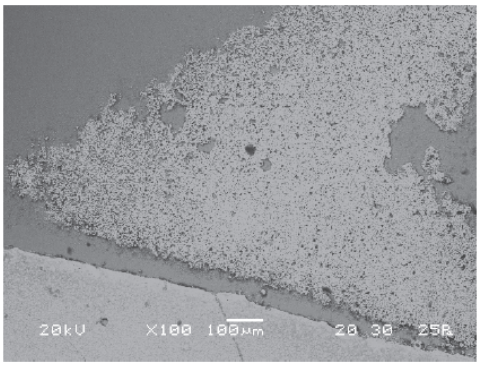

Figure 4.5: SEM image of the sample 400 °C-4 h, magnification 100X; on the top of the image the dipped part of the sample and in the bottom the not dipped part.

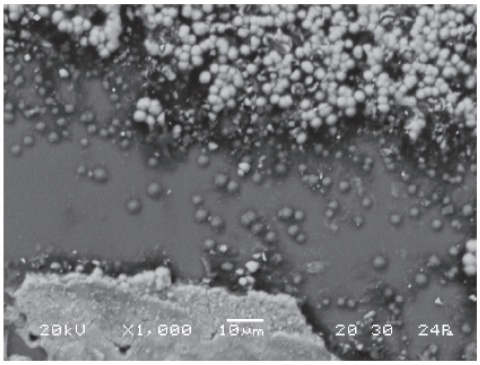

Figure 4.6: SEM image of the sample 400 °C-4 h, magnification 1000X; on the top of the image the dipped part of the sample and in the bottom the not dipped part.

The presence of 'salt islands' represents a negative feature for the application of the doped PV panel as LDS because they lower the surface optical quality and also they could partially avoid the Cu ions penetration inside the matrix. The optical absorption spectra for some Cu-doped samples obtained by ion exchange in CuCl:$ZnCl_2$ are reported in figure 4.7. As it can be observed, only a red shift of the glass cut-off and a small increasing of optical density over 350 nm are noticeable; these features show that the copper seems to be mostly present in 1+ oxidation state. The higher absorption recorded at higher wavelengths for the sample exchanged at 400 °C can be associated to the light scattering from the salt islands before discussed.

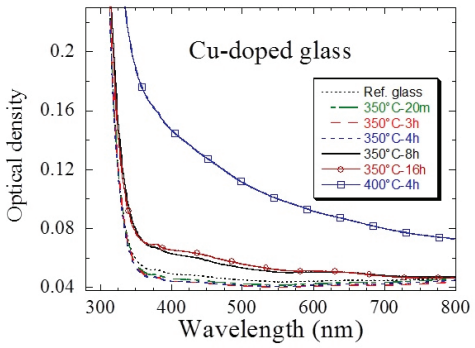

Figure 4.7: Optical absorption of cover glass doped by CuCl:$ZnCl_2$ bath.

The fluorescence spectra recorded with λ_{exc} =260 nm are reported in figure 4.8 l a; all the PL spectra show the Cu^+ ions green emission band (peaked around 500 nm) to whom corresponds an excitation band around

250-310 nm in the PLE analyses (figure 4.8 b). For exchange times higher than few hours, the PL intensity decreases and the absorption increases probably due to the quenching effect generated by the presence of bivalent Cu ions [150].

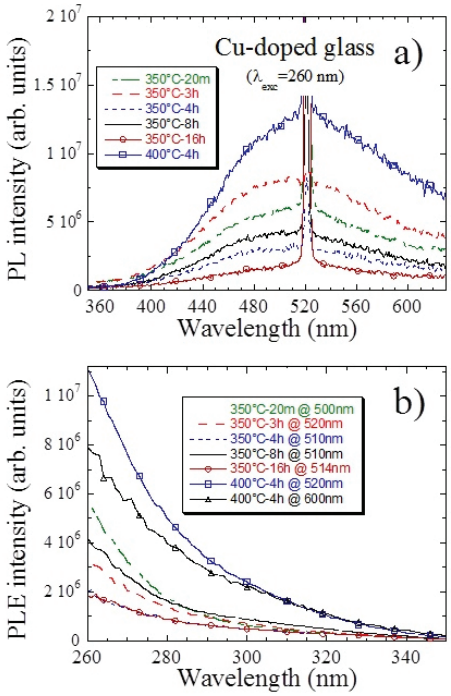

Figure 4.8: PL spectra (panel**a**, $\lambda_{exc.}$= 260 nm) and PLE spectra (panel**b**, $\lambda_{emis.}$= 510 nm) of cover glass doped by CuCl:$ZnCl_2$ salt bath. The sharp peak close to $2\lambda_{exc.}$ in the PL spectra is an unfiltered spurious signal due to the Xe lamp.

Recording the PL spectra using a light of 340 nm for excitation (figure 4.9) only the sample exchanged at 400 °C and the glass doped at 350 °C and annealed at 500 °C for 1 h show an emission band centered around 600 nm. This band can be related to the presence of copper pairs, as discussed before..

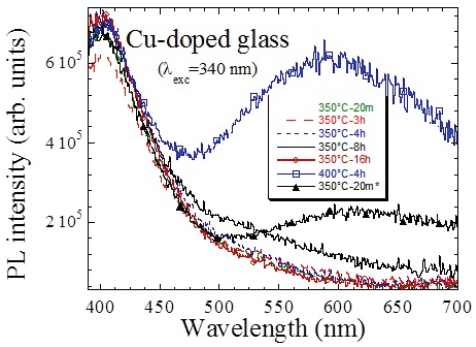

Figure 4.9: PL spectra (λ_{exc}= 340 nm) of cover glass doped by floating in CuCl:$ZnCl_2$ salt bath.

So, it can be concluded that high process temperatures promote the formation of copper dimers. Considering the luminescence trend recorded, the best condition for the copper emission seems to be the realization of exchange of short duration.

4.7.3 X-ray Absorption Spectroscopy (XAS) analysis

The samples doped by CuCl:$ZnCl_2$ bath have been studied by XAS analysis in order to investigate the copper oxidation states. Soda-lime glasses doped with CuCl:$ZnCl_2$ and studied by XAS were previously described by Lee et al [156]. After few days of doping they found the copper mostly under the monovalent state and the coordination number was found to be variable, in same case similar to Cu^{2+} ion. XAS analyses of soda-lime glasses doped with a $CuSO_4$:Na_2SO_4 were done too. By taking advantage of the grazing incidence approach, it has showed that the Cu^+/Cu^{2+} ratio is not constant along the exchange layers; in particular the Cu^{2+} ions resulted concentrated mainly inside the first layers of the exchanged glass [157]. Maurizio et al. showed that the Cu^+ characteristic pre-peak XAS intensity can be influenced by the O−Cu−O angle [158]. The X-ray absorption near edge structure (XANES) spectra of the four samples analyzed are reported in figure 4.10; in the same picture the XANES spectra of the Cu, CuO and Cu_2O standards are included. Observing the evolution of the recorded profile it is possible to notice a modification of the Cu K-edge with the increasing of the exchange duration.

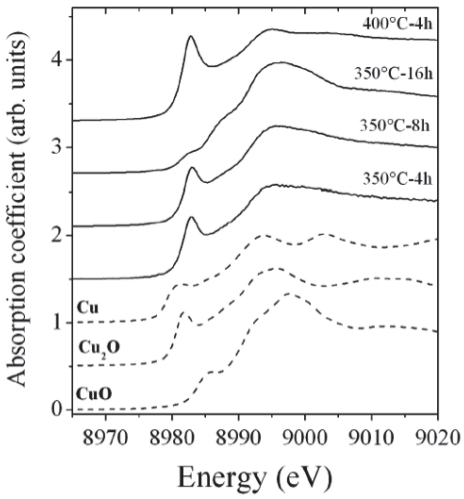

Figure 4.10: Cu K-edge XANES spectra of copper doped PV panels obtained by CuCl:$ZnCl_2$ bath.

The pre-peak placed at 8982 eV (focusing on the spectra of Cu_2O standard) is characteristic of Cu^+ ions. This signal is clearly visible for the sample 350 °C-4 h and then it decreases with the increasing of the duration of doping. Furthermore, the spectra recorded have been simulated with a linear combination of the standard XANES profiles as proposed for instance by Gonella et al. [157]; this operation lets us to do an evaluation of the ratio between the different oxidation state of the dopant ions inside the doped glass. The results are resumed in the following table (table 4.2).

	$\mathbf{Cu^0}$	$\mathbf{Cu^+}$	$\mathbf{Cu^{2+}}$
350 °C-4 h	<0.2	0.6-0.8	0.1-0.3
350 °C-8 h	<0.2	0.5-0.7	0.2-0.4
350 °C-16 h	<0.1	0.2-0.4	0.6-0.8
400 °C-4 h	<0.2	>0.8	<0.1

Table 4.2: Cu oxidation state fractions evaluated form the K-edge XANES simulation.

It can be noticed that, by increasing the process duration, the amount of Cu^{2+} increases at the expense of the Cu^+ ions, while if the exchange tem-

perature is increased an opposite trend occurs. In spite of the presence of copper in the +2 oxidation state, the absence of Cu^{2+} optical absorption band (in the optical absorption spectra of the 350 °C samples) is consequence of the small total amount of dopant ions in our glass (the total amount of copper inside our 350 °C samples is lower than 10^{17} atoms/cm^2, as obtained by RBS data).

4.8 Solar cell power measurements

The capability of the doped PV panels to act as a LDS has been tested by the measurement of the output power of a solar cell covered by the doped glasses and illuminated with a solar simulator. For the samples proposed until now the I vs V test has been collected by a solar simulator (Abet technologies-sun 2000) located at the "Legnaro National Laboratories (LNL)-INFN" equipped with a GaAs small solar cell (fill factor 0.77). Some examples of the most representative samples are showed in figure 4.11.

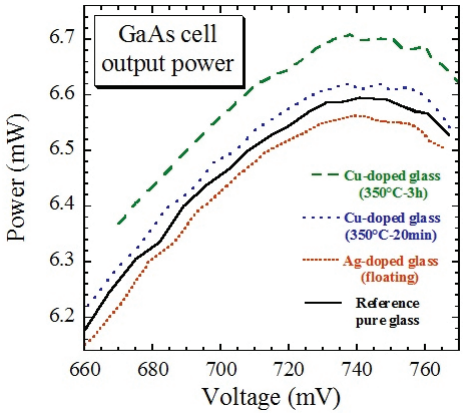

Figure 4.11: Comparison between the power produced by PV cell covered by some glasses doped with Ag (floating) and with Cu-doped glasses (CuCl:$ZnCl_2$ bath).

Focusing on the silver doped glasses, the dipped and the annealed samples gave poor results if compared to the untreated glass. That can be justified on the basis of the marked optical absorption in the visible region generated by the tin oxo-reduction action that promotes the silver precipitation to form nanoparticles (for the dipped glass) and by the annealing induced silver aggregation. The floated slide gives the best result despite the mea-

sured power is slightly lower than for the untreated glass. For the samples exchanged with CuCl:$ZnCl_2$ salt bath, the two best performing were resulted to be the 350 °C-20 min and the 350 °C-3 h: for this last the increment of the maximum output power with respect to the virgin PV glass is of 2%. The Cu-PV panels exchanged for times longer than 3 h, give rise to curves comparable to the reference one within the experimental errors. In fact for these samples the XANES analyses showed the increasing of the Cu^{2+}/Cu^{+} fraction: the quenching effect of the Cu^{2+} presence on the Cu^{+} emission could be the principal reason for this result [159]. The samples doped at 400 °C for 4 h increased the output power no more than the 350 °C-20 min sample, even if the dopant species seems to be present mainly as Cu^{+}. The reason for this result could be found on the presence of salt islands that reduces the optical quality of the sample surfaces, thus increasing the light scattering.

4.9 General considerations

From this preliminary study it results that both silver and copper doped glasses (exchanged by CuCl:$ZnCl_2$) are able to realize the down-shifting conversion of light. Despite that, in case of silver doped glasses the reduction of the dopant and the precipitation of silver nanoparticles are the major drawbacks because they increase the visible absorption. The photoluminescence quantum yield (PLQY) was measured for the as-exchanged glass realized by floating; due to the small signals recorded, it was estimated an upper limit for the PLQY close to the 0.5% (λ_{exc}=280 nm). The copper doped glasses are promising too. In this case the presence of cupric ions resulted to be the limiting parameter owing to its capability to quench the green emission of cuprous ions. The PLQY has been evaluated also for the glass doped with copper at 350 °C for 3 h; the PLQY is $\leq$ 0.4 % (λ_{exc}=280 nm). With the aim to continue the study about the application of TM doped glasses by ion exchange for down-shifting application, the key role point seems to be the increasing of copper concentration avoiding the cupric ions formation. For that CuCl:$ZnCl_2$ seems to be the most suitable salt bath but it is important to preserve the optical quality of the glass surfaces too. About the silver, the most promising method seems to be the control of the luminescent species formation, on the meantime avoiding the nanoparticles formation. The study

has been then continued following these directions. In particular, in the following a study about the optimization of the luminescence silver properties is presented. About the copper, being one of the most interesting samples the glass exchanged at 400 °C due to its intense emission and low presence of Cu^{2+} ions, it has been chosen to explore this temperature with the aim of improving the dopant concentration and the green luminescence, being aware of the surface quality.

CHAPTER 5

Silver doped silicate glasses for solar cells covering

One of the most recently published paper on silver doped glasses was done by Simo et al. [53]. In this work they studied the growth mechanism of silver aggregates inside Ag-doped silicate glass. They showed that the cluster formation is mainly affected by two factors: the annealing conditions after the ion exchange and the number of the non bridging oxygens (NBOs) in the glass structure. The control of the average size of the silver aggregates is actually devoted to temperature and time of the post-synthesis thermal treatment, while the NBOs have the task of reducing agent for the silver ions. Moreover, one of the most interesting evidence they have taken out by their research is the existence of a threshold annealing temperature to whom the growth process and the final dimension of the silver aggregates depend. They found for their Ag-doped silicate glass the threshold annealing temperature to be 410 °C. Below 410 °C, the formation of molecular cluster of diameter less than 1 nm, mainly dimers or trimers, was observed; these molecular clusters are stable inside the glass matrix and do not dissolve. Above the threshold temperature, the grown of nanoparticles of size larger than 1 nm is attained.

In the previous pages, a starting study of silver doped glasses for down-shifting application is reported. From the preliminary attempts, the silver showed to possess the right luminescent properties but the major drawback resulted to be the high absorption of the doped glasses, mainly related to the

formation of silver nanoaggregates. Considering what has been proposed by Simo et al. [53], the determination of the threshold temperature T_{th} for our Ag–doped glasses could be the right way to maximize their down–shifting properties by a suitable thermal treatment after the ion exchange. In fact by carefully controlling the thermal treatment after the doping, a better control of the glass luminescence and absorption can be achieved by increasing the formation of silver dimers, trimers and very small clusters, and by avoiding high concentrations of silver nanoaggregates, these lasts detrimental to the glass transparency due to their well known surface plasmon resonance (SPR) absorption band centred around 400 nm of wavelength. So, the aim of the following approach is to look for the right conditions (Ag salt bath concentration, post–synthesis annealing temperature and duration time) to obtain the most useful down-shifting properties. To do this, tin-free soda-lime glasses were used to avoid the tin influence on the dopant redox state; the composition of the glass is reported on table 5.1.

Component	**Atomic %**
O	59.6
Si	23.9
Na	10.2
Ca	2.4
K	0.5
Mg	2.6
Al	0.8
Ti	traces

Table 5.1: Composition of the soda-lime glass used in this study.

5.1 Experimental

Ag^+-Na^+ ion exchanges were performed by dipping soda-lime slides inside a molten salt bath of $AgNO_3$:$NaNO_3$ (1:99) for 1 h at the temperature of 320 °C. Moreover, some soda-lime slides were doped by dipping inside $AgNO_3$:$NaNO_3$ mixture concentrated at the 0.1% mol. of $AgNO_3$; the exchange temperature and the duration were unchanged. After the doping

the doped glasses were thermal treated in air at the temperature of 380 °C, 410 °C or 440 °C; for each temperature of annealing three different duration were explored: 1 h, 4 hours and 16 hours. After that the samples have been studied by optical absorption, photoluminescence spectroscopy and by the P vs V cell test.

5.2 Characterization and results

5.2.1 $AgNO_3$:$NaNO_3$ 0.1% mol. bath

The optical absorption spectra are reported in figure 5.1; as it can be seen, not particular absorption bands are present probably due to the low amount of silver inside the glass.

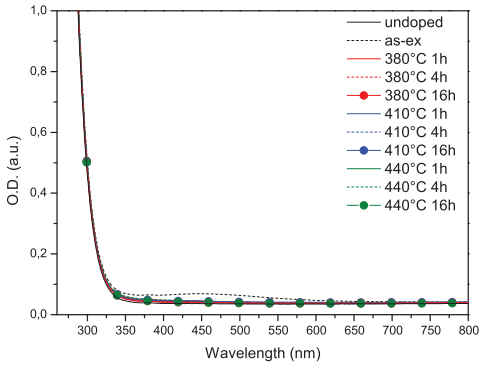

Figure 5.1: Optical absorption spectra of soda-lime glasses doped by $AgNO_3$:$NaNO_3$ 0.1% mol. salt bath and thermal treated.

The luminescent study of the samples has been done under similar conditions already used and reported for the same analyses presented in the previous chapter. Exciting the samples with a wavelength of 260 nm, the characteristic emission generated by the presence of the Ag^+-Ag^+ pairs was detected (figure 5.2). The highest intensity is recorded for the as-exchanged sample; after the annealing the emission band changes in intensity and position too. It is interesting to note the maximum of the emission results blue-shifted with the increase of the temperature of annealing and/or increasing the treatment duration.

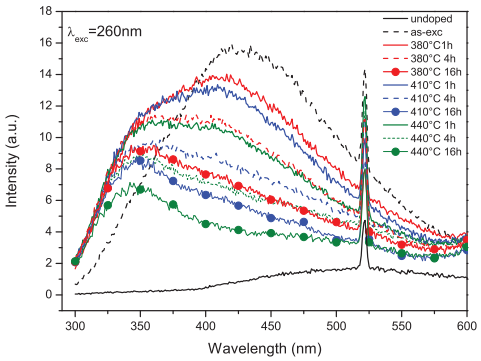

Figure 5.2: Emission spectra of soda-lime glasses doped by dipping in $AgNO_3$:$NaNO_3$ 0.1% mol. salt bath and thermal treated; λ_{exc}= 260 nm. The sharp peak close to $2\lambda_{exc.}$ in the PL spectra is an unfiltered spurious signal due to the Xe lamp.

The highest intensity is recorded for the as-exchanged sample; after the annealing the emission band changes in intensity and position too. It is interesting to note the maximum of the emission results blue-shifted with the increase of the temperature of annealing and/or increasing the treatment duration. The band detected is placed around 350 nm and can be ascribed to isolated silver ions. This could be due to a decrease of the surface silver concentration as a consequence of diffusion phenomena introduced by the thermal annealing. The related PLE spectra (figure 5.3) show the Ag absorption band under 350 nm and mainly concentrated under 300 nm.

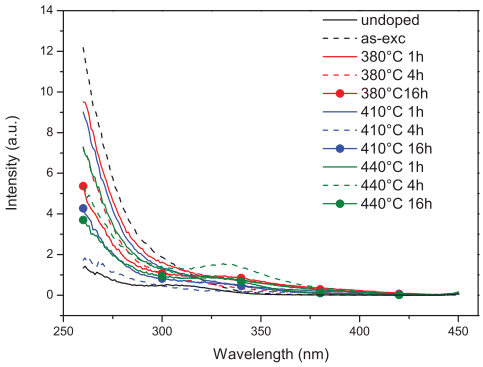

Figure 5.3: Excitation spectra of soda-lime glasses doped by dipping in $AgNO_3$:$NaNO_3$ 0.1% mol. salt bath and thermal treated ($\lambda_{emis.}$= 450 nm, blue band).

The orange emission trend collected under λ_{exc} =350 nm is resumed

in figure 5.4; in this case the band is placed close to 500 nm. Generally speaking the glasses treated for 4 hours show the best intensity, moreover the highest intensity is recorded for the sample 410 °C-4 h. Differently, the glasses treated for 16 h show the less intense signals. PLE analyses (figure 5.5) are characterized by the presence of the absorption band between 350 nm and 400 nm. This band shows the same trend intensity of the PL orange band.

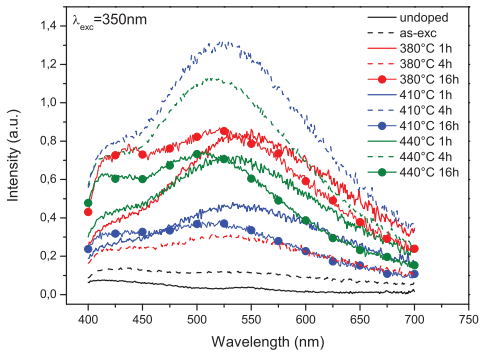

Figure 5.4: Emission spectra of soda-lime glasses doped by dipping in $AgNO_3$:$NaNO_3$ 0.1% mol. salt bath and thermal treated; $\lambda_{exc.}$= 350 nm.

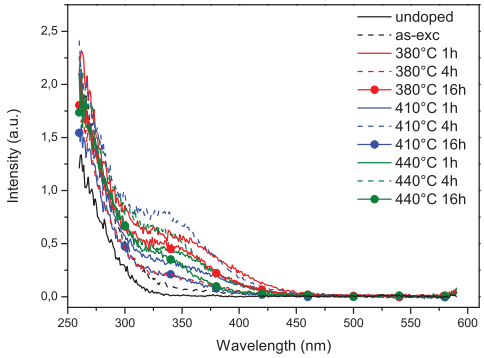

Figure 5.5: Excitation spectra of soda-lime glasses doped by dipping in $AgNO_3$:$NaNO_3$ 0.1% mol. salt bath and thermal treated ($\lambda_{emis.}$= 550 nm, orange band).

5.2.2 $AgNO_3$:$NaNO_3$ 1% mol. bath

The optical absorption evolution as a function of the annealing parameters is reported (figure 5.6); from the as–exchanged sample, the changes

are more marked for annealing at higher temperatures as well as at longer times. The glasses treated at 380 °C are characterized by an absorption band located around 350 nm; this feature could be related to the absorption by sub-nanometric silver multimeric complexes [53] [160]. At 410 °C the same absorption band around 350 nm was found; in this case the most intense absorption is observed for the sample treated for 4 h indicating the highest formation of absorption species obtained with this treatment. The glasses treated at 440 °C are the most absorbing samples and the absorption increases in intensity by increasing the annealing duration, indicating the progressive formation of silver aggregates inside the samples; the presence of small nanoparticles could not be neglected due to the faint slope changing over 400 nm in case of 440 °C-16 h.

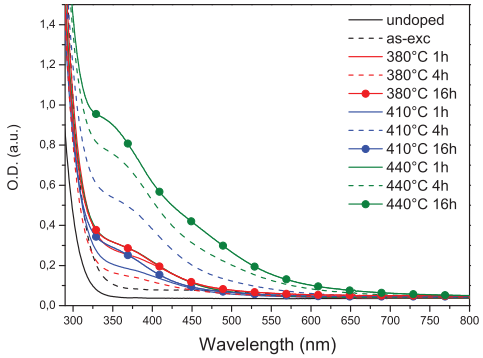

Figure 5.6: Optical absorption spectra of soda-lime glasses doped by $AgNO_3$:$NaNO_3$ 1% mol. salt bath and thermal treated.

In the perspective to use these glasses as cover for PV cells, a good transparency is required: for that, the worst samples seem to be those treated at 440 °C for the longer times and the 410 °C for the medium time.
The luminescence spectra obtained at λ_{exc}=260 nm show the typical blue emission of Ag^+-Ag^+ pairs. The samples series treated at 410 °C is the only one showing an increasing of blue band intensity with the annealing duration, and the sample treated for 16 h shows the most intense emission (figure 5.7). The PLE spectra related to the blue emission (figure 5.8) evidence that the silver pairs absorb mainly under 400 nm and in particular for the samples 410 °C-16 h, 440 °C-16 h, 440 °C-4 h and 380 °C-16 h an absorption peak is clearly noticeable around 350 nm.

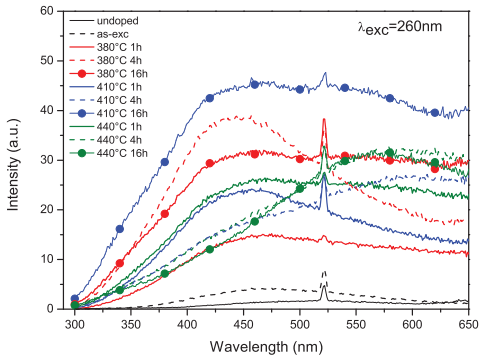

Figure 5.7: Emission spectra of soda-lime glasses doped by dipping in $AgNO_3$:$NaNO_3$ 1% mol. salt bath and thermal treated; $\lambda_{exc.}$=260 nm. The sharp peak close to $2\lambda_{exc.}$ in the PL spectra is an unfiltered spurious signal due to the Xe lamp.

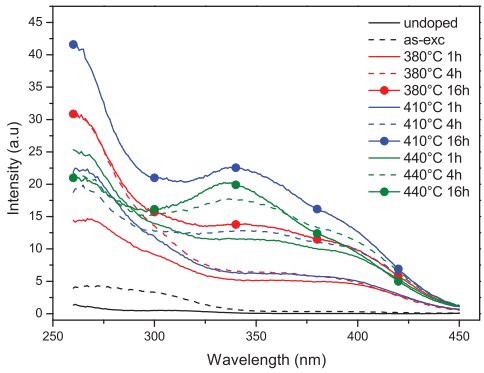

Figure 5.8: Excitation spectra of glass doped by dipping in $AgNO_3$:$NaNO_3$ 1% mol. ($\lambda_{emis.}$= 450 nm, blue band).

Using an excitation wavelength of 350 nm it has been recorded the orange emission (charged silver multimers); also in this case the 410 °C series is characterized by a trend different form the other two series and, as observed in case of blue emission, the doped glass treated for the longest time shows the highest intensity (figure 5.9). From the PLE spectra the absorption related to orange band result placed under 400 nm but a faint absorption is presence well above 400 nm; the most absorbing samples are the 440 °C-16 h and the 410 °C-16 h (figure 5.10).

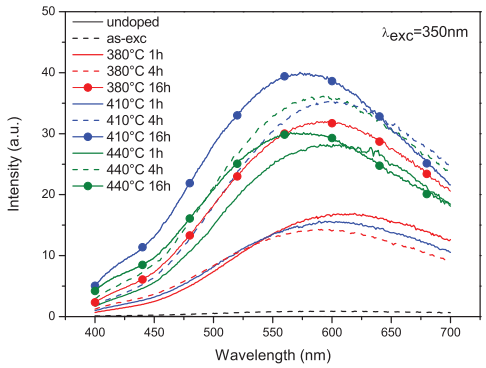

Figure 5.9: Emission spectra of soda-lime glasses doped by dipping in $AgNO_3$:$NaNO_3$ 1% mol. salt bath and thermal treated; $\lambda_{exc.}$=350 nm.

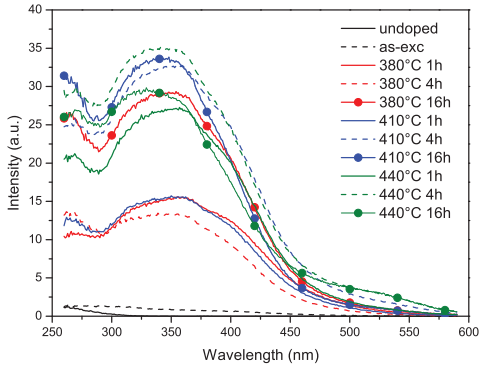

Figure 5.10: Excitation spectra of soda-lime glasses doped by dipping in $AgNO_3$:$NaNO_3$ 1% mol. salt bath and thermal treated ($\lambda_{emis.}$= 600 nm, orange band).

5.3 Photoluminescence quantum yield measurements

Table 5.2 summarizes the PLQY values measured at λ_{exc}=350 nm (recorded emission in the 380–750 nm region) for the most interesting samples doped with the 1 % mol. silver bath.

Silver bath	Treatment	PLQY
0.1 %	440°C 4 h	5%
1 %	as-exc.	2 %
1 %	380°C 4 h	17%
1 %	410°C 1 h	14%
1 %	410°C 4 h	8%
1 %	410°C 16 h	26%
1 %	440°C 1 h	13%

Table 5.2: Photoluminescence quantum yield measured at $\lambda_{exc.}$= 350 nm.

Starting from the as–exchanged glass (PLQY about 2%) the subsequent thermal treatments help to increase the PLQY as a consequence of the formation of the useful Ag luminescent aggregates. At the annealing temperature of 380 °C, the most interesting samples is the 380 °C–4 h (PLQY 17%) suggesting that at this temperature the formation of large silver aggregates is prevented, thus favoring the anyways slow formation of silver dimers, trimers, and small multimers. The samples annealed at 410 °C exhibit a marked increase of the PLQY showing once again that the best–performing sample is obtained after 16 h of annealing. For this series of samples the 410 °C–4 h exhibits again an unclear behaviour; the low PLQY recorded could be associated to the presence of important auto–absorption phenomenon. The silver doped glass treated at 440 °C-1 h shows a interesting improvement of PLQY; in this case the shortness of the thermal treatment induces the formation of the "right" Ag aggregates without significant formation of larger silver precipitates, which are detrimental due to their high absorption and low emission. About the samples exchanged with the less silver concentrate bath, only the glass treated at 440 °C-4 h has been analyzed; the PLQY is very low probably suggesting once again the dopant concentration is too low to permit an useful light conversion.

5.4 Solar cell power measurements

Taking into account the experimental findings, we expect that the best performance of our glasses should be obtained by the samples that showed the highest PL emission intensity and, on the meantime, the lowest absorption: the best–performing sample is expected to be the 410 °C–16 h. The performance of the Ag–doped silicate glasses as PV cell cover was evaluated by the setup acting as a solar simulator described in the chapter 2. Placing the doped slides on the Si solar cell the output power has been extracted from the I vs V measurement. The results are summarized in figures 5.11 and 5.12.

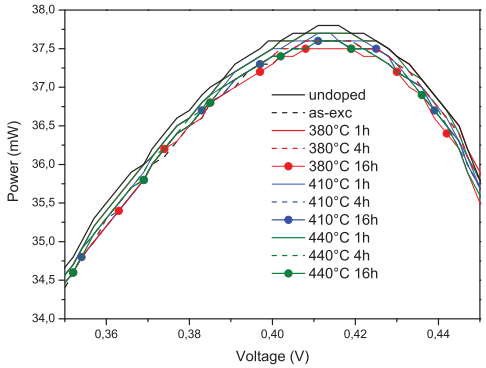

Figure 5.11: Power produced by soda-lime glasses doped by $AgNO_3$:$NaNO_3$ 0.1% mol. salt bath and thermal treated.

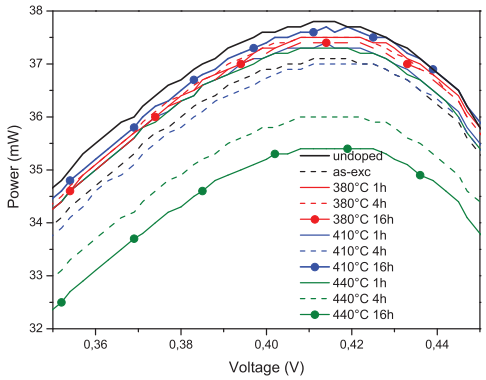

Figure 5.12: Power produced by of soda-lime glasses doped by $AgNO_3$:$NaNO_3$ 1% mol. salt bath and thermal treated.

The obtained curves show that up to now none of the Ag–doped glasses

is able to increase the cell yield; in fact, the output power is always less than the power produced by the cell covered with the undoped glass. The worst results have been obtained for the samples treated at 440 °C for the longest times, and the 410 °C–4 h one. About the firsts two, the bad behaviour is probably related to high absorption showed by these samples due to a notable formation of sub–nanometric silver aggregates (i.e., made of more than few atoms): these structures are strongly absorbing, inducing a loss of transparency without a significant down-shifting effect. About the 410 °C–4 h sample, its behaviour is really unclear and it needs additional investigations. As far as the other samples, they show a similar behaviour: probably, the annealing treatment cannot increase significantly the formation of silver luminescence aggregates. At last the best-performing, as expected, is the sample annealed at 410 °C for 16 hours.

5.5 Discussion

What appears by the characterization exposed is that up to now the power produced by the cell when the doped and annealed glasses are used as covers is close to the power produced with the undoped glass. The results obtained by the luminescent study could be interpreted assuming the coexistence of two different processes activated by the thermal treatment: the dilution effect due to the silver diffusion through the matrix and the growth of silver luminescent aggregates. Referring to the samples exchanged with the 0.1% Ag bath, the amount of dopant ions inside the glass is limited. Probably as a consequence of the low silver concentration, during the annealing the diffusion counteracts the formation of silver aggregates and it becomes the most important phenomenon. The presence of the UV emission of isolated silver ions on the PL spectra (λ_{exc}=260 nm) support this hypothesis. In the case of glasses exchanged with the 1% Ag bath and treated at 380 °C and 440 °C the blue emission (silver pairs) and orange emission trend show an improvement of the emitted light with the increasing of annealing time from 1 h to 4 h and then a decrease is recorded. Differently, the PL emissions from the glasses treated at 410 °C grows up with the time of annealing. At 380 °C the formation of the first luminescent silver aggregates takes place; the increasing of the PL intensity from 1 h to 4 h of treatment at 380 °C is due to the rising of the luminescent species number. Differently, the reason for the

decrease of the PL intensity recorded in case of the sample treated for the longest time (380 °C-16 h) could be justified by considering concentration quenching mechanisms of the luminescent emission. Concentration quenching is a phenomenon observed in organic and inorganic system, consisting on the decrement of the emission intensity when the luminescent centers concentration is above a critical value [161]. This phenomenon has been widely studied; despite a general explanation does not exist yet, the principal processes invoked to justify this type of quenching are: formation of luminophor aggregates with not luminescent properties (nonluminescent polymers), collisional quenching between luminescent species, non-radiative energy transfer between an excited species to an unexcited one separated by large distance, and resonance energy transfer between luminophores (fluorescence resonance energy transfer, FRET [162]) [163] [164]. In general, these theories have in common that the quenching needs a reduced distance between luminescent centers to occur, condition verified when the centers concentration is high [161] (or when the interaction between fluorophores is diffusion-controlled [165]). Probably in case of 380 °C-16 h sample, the thermal treatment duration increases the formation of luminescent silver aggregated but - at the same time - the low temperature makes the ions diffusion very slow. Being the luminescent species concentrated in a small portion of sample volume, it is possible to assume that the condition of proximity among luminescence centers is attained and the quenching can occur. At 440 °C the temperature is sufficiently high to induce the formation of the first silver precipitates (probably over 1 nm in size) that do no possess luminescent properties. In fact, for these samples the optical absorption analyses showed an increment of optical density over 410 nm (the starting seed of the SPR band of the silver nanocluster). The temperature of 410 °C seems represent the best condition to that corresponds the best equilibrium between the formation of luminescent aggregates and dilution effect (this last decreasing the probable quenching effects). Although the PLQY analyses were collected only for a small number of samples, the results appear to be in agreement with this hypothesis.

In order to estimate the right value of the T_{th} of the exchanged samples, a statistical fitting approach has been used (Statistica 8.0) to study the possible variation of PL emission. This was done by referring to the orange emission (λ_{exc}=350 nm; wavelength recorded range: 400-700 nm). The PL

area of the spectra recorded as a function of the t and T values has been evaluated; this was done only for the 9 annealed samples after doping with 1% silver bath. The intensity obtained I(t,T) has been fitted by using a spline smoothing fit type. In figure 5.13, the 2D projection of the 3D simulated surface is reported; from the simulation the most promising annealing conditions to maximize the 350 nm PL emission should be a temperature in the range 405–420 °C, for duration times in the range 9–12 hours. Although the experimental points are limited in number and not homogeneously distributed in the (t,T) plane, the obtained estimations are in agreement with the experimental findings reported above.

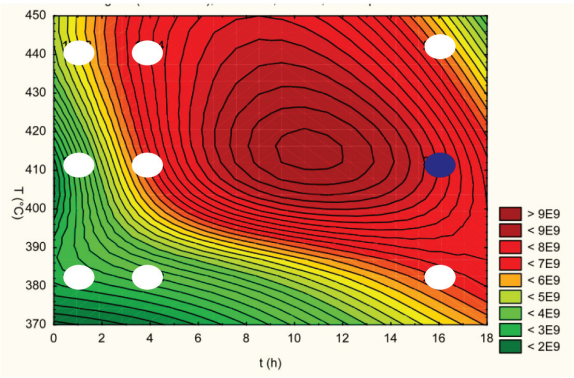

Figure 5.13: 2D projection of the 3D simulated surface plot; the white circles represent the experimental points and the blue circle the best-performing sample (410 °C-16 h).

Similar fits made with other smoothing functions (such as the distance-weighted least square and the negative exponential smoothing) gave comparable results. Starting from these suggestions, the prosecution of this work could be a more refined experimental investigation in the suggested (t,T) best-region, made for instance by the realization of additional thermal treatments of the as-exchanged 1% glass, with steps of 5 °C for T and of 30 min. for t.

5.6 Conclusions

In this study it has been tried to determine the most favourable annealing temperature for Ag–doped soda–lime glasses to improve the luminescent emission and to reduce as much as possible the formation of VIS-absorbing aggregates. To do that, the photoluminescence properties of the silver doped glasses have been studied after thermal treatments in air at different temperatures and duration times. The luminescent trends have been interpreted assuming that two processes occur: the diffusion of dopant ions and the growth of nanoaggregates. These two processes can occur with different importance, in relation to the dopant concentration and the annealing conditions. In particular, for the less concentrated samples the dilution of the matrix seems to be the most enhanced effect. In the samples exchanged with the most concentrated silver bath, the growth of luminescent aggregates is prevailing, thus inducing the best luminescent properties for the sample annealed at 410 °C for 16 h. The study of the PLQY seems to confirm these results. The samples were used then as cover of a Si cell in our home-made solar simulator to easily check their performances; none of the Ag–doped glasses showed a detectable increase of the output power. Considering all the results obtained, the reported range for the post–synthesis annealing (405–420 °C for the temperature, 9–12 hours for the time) could allow the production of best–performing Ag–doped samples. In the next future these conditions will be investigated, with more refined T and t steps (5 °C and 30 min., respectively).

CHAPTER 6

Copper doped silicate glasses for solar cells covering

In the chapter 4 two different copper salt mixtures were studied to dope the PV glass panels with the aim to induce down-shifting phenomena. The first salt bath used was a $CuSO_4$:Na_2SO_4 mixture (45:55); after the exchange process the glasses resulted coloured and characterized by high absorption in the UV-VIS range due to the presence of copper nanoparticles. These features are detrimental for the solar application of the doped glasses and for that the sulphate salt bath has been discharged. More encouraging results were obtained doping the PV panels with the CuCl:$ZnCl_2$ bath (11:88); in this case an improvement of the solar cell maximum output power has been detected. On the basis of the optical properties (absorption and photoluminescence) and of the Cu^{2+} presence revealed by the XAS measurements, it has been concluded that the best condition for doping the PV panels with copper is to realize the ion exchange at 400 °C for medium duration (4 h). Starting from this point, the aim of the study reported hereinafter is to dope the PV glass panels by improving the Cu^{+} ions concentration and reducing as much as possible the Cu^{2+} ions concentration; acting in this way it could be possible to enhance the luminescence properties of the dopant and the spectral conversion too. For that the exchange temperature of 400 °C has been studied. To avoid the formation of the Cu^{2+} ions, the exchange duration lower than 4 hours has been taken into account; moreover the less dipping time inside the bath and the stirring action of the bath should avoid

the salt islands formation on the glass surface.

6.1 Experimental

PV cover glass panels (composition is reported on table 4.1) were doped with copper by thermal ion exchange process. The glasses were dipped inside a 11:89% mol. (eutectic concentration) CuCl:$ZnCl_2$ (**CuZn**) fused bath at the temperature of 400 °C for 20, 80 and 320 minutes. The copper bath was fused inside a ceramic crucible and the samples were dipped holding the tin contaminated face oriented towards the external part of bath; the stirring of melt has been manually done by a glass stick every 15 minutes. Moreover a new type of salt mixture was studied too. PV cover glasses have been doped by dipping inside a CuCl:NaCl 74.5:25.5% mol. (**CuNa)** eutectic mixture at the temperature of 400 °C for 20, 80 and 320 minutes of exchange; the exchanges were carried out under the same experimental condition used for CuZn bath.
After the exchange the sample were analyzed by RBS, optical absorption and photoluminescence spectroscopy and by recording the I vs V cell curve to measure the solar cell yield covered by the exchanged samples.

6.2 Results

6.2.1 CuCl:$ZnCl_2$ salt bath

The diffusion profile of copper inside the glasses doped by CuCl:$ZnCl_2$ is reported on figure 6.1; increasing the exchange time the penetration depth becomes greater and the shape of distribution profile changes. In the sample doped for the shortest time the copper is concentrated immediately under the surface and its relative atomic concentration is about 1.3%. After 80 minutes of exchange, the first 100 nm below the glass surface resulted depleted of dopant; the highest copper concentration is reached at about 300 nm in depth and it is close to 0.5 atomic %.

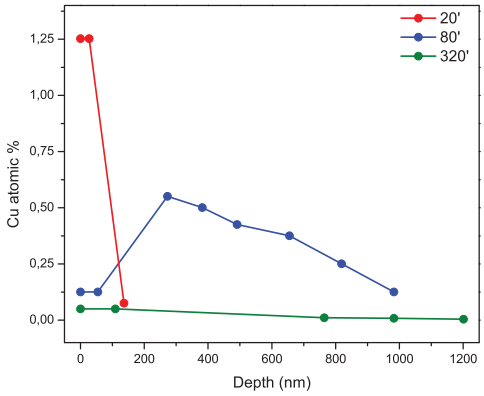

Figure 6.1: Copper diffusion profile inside PV cover panels doped by CuCl:$ZnCl_2$ fused bath for different time as obtained by RBS measurement. The relative uncertainty on the concentration values is of 10%.

In the sample exchanged for the longest time the concentration of copper below the surface is the lowest and it decreases from the surface towards the bulk following an almost flat distribution; in this case copper seems to be diffused over 1 μm in depth. At last for every samples the dynamic of exchange is compatible with:

$$1\,Cu^{+}_{bath} \leftrightarrows 1\,Na^{+}_{glass}.$$

The figure 6.2 reports the optical spectra of the copper doped panels; the exchanged glass spectra are shifted along the optical density axis probably due to light scattering phenomena by the surfaces. At the lowest wavelength (around 400 nm) the absorption seems to increase respect to the undoped glass; this increment could be associated to the presence of Cu^{+} ions.

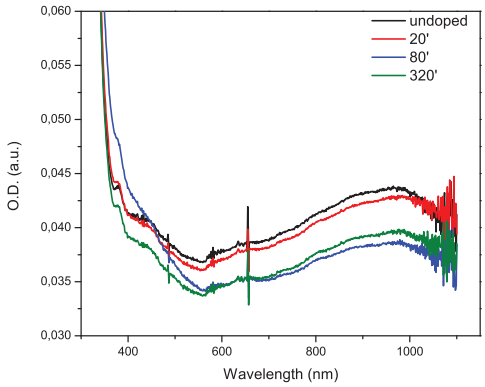

Figure 6.2: Optical absorption spectra of PV cover panels doped by CuCl:$ZnCl_2$ fused bath for different time.

On figure 6.3 the photoluminescent analysis under an excitation wavelength of 260 nm is reported. The virgin glass shows two emission bands at 450 nm and 510 nm and after the exchange an increasing of the emission bands is recorded due to the typical green emission of cuprous ions in the matrix.

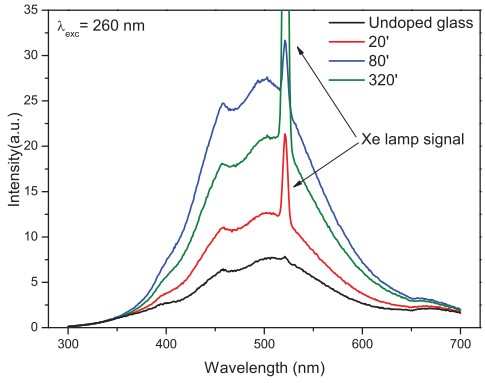

Figure 6.3: Emission spectra of PV cover panels doped by CuCl:$ZnCl_2$ fused bath for different time; $\lambda_{exc.}$= 260 nm. The sharp peak close to $2\lambda_{exc.}$ in the PL spectra is an unfiltered spurious signal due to the Xe lamp.

The excitation spectra were collected at both emission maximum observed on the emission spectra (457 nm and 510 nm respectively) (figures 6.4 and 6.5). In both cases, the absorption profile shape is not changed by the exchange process but the absorption intensity is increased mainly under 320 nm by the Cu^+ ions absorption. This result confirms the association between the improvement of the emission observed and the green emission

of Cu^{+} ions in the matrix; moreover the absorption and the emission spectra follow the same trend.

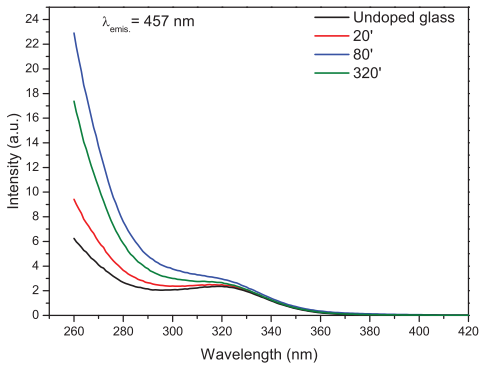

Figure 6.4: Excitation spectra of PV cover panels doped by CuCl:$ZnCl_2$ fused bath for different time; $\lambda_{emis.}$= 457 nm.

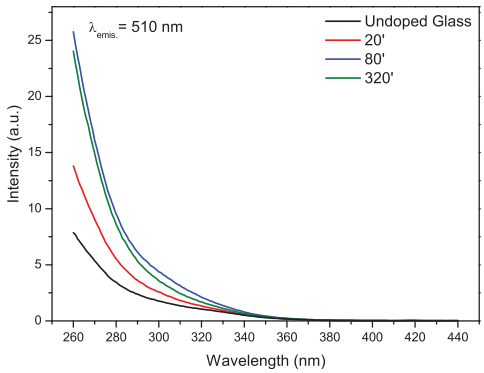

Figure 6.5: Excitation spectra of PV cover panels doped by CuCl:$ZnCl_2$ fused bath for different time; $\lambda_{emis.}$= 510 nm.

The luminescence properties were also studied using an excitation of 350 nm with the aim of verifying the presence of copper pairs (orange band). As it can be seen (figure 6.6), no particular emission band was recorded at least of a weak gain over 600 nm to that correspond absorption profiles similar to ones recorded for the emission at 510 nm (figure 6.7).

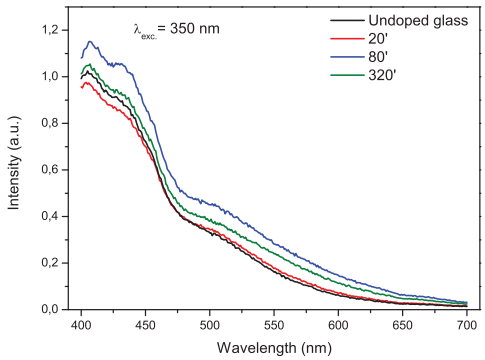

Figure 6.6: Emission spectra of PV cover panels doped by CuCl:$ZnCl_2$ fused bath for different time; $\lambda_{exc.}$= 350 nm.

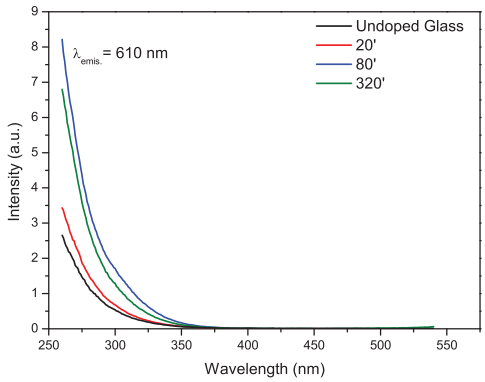

Figure 6.7: Excitation spectra of PV cover panels doped by CuCl:$ZnCl_2$ fused bath for different time; $\lambda_{emis.}$= 610 nm.

6.2.2 CuCl:NaCl salt bath

The copper distribution inside the glasses doped by CuCl:NaCl salt mixture is reported in figure 6.8. The maximum copper concentration is always reached inside the first layers under the surface and the quantity of dopant increases with the time of exchange. As already seen for the samples dipped in the CuZn mixture the exchange process involves the diffusion of copper ions from the bath and the sodium ions of the glass in ratio of 1:1.

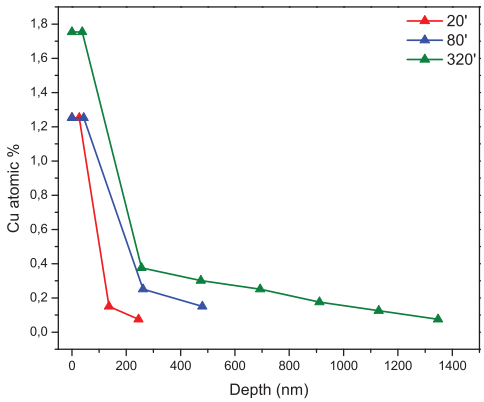

Figure 6.8: Copper diffusion profile inside PV cover panels doped by CuCl:NaCl fused bath for different time as obtained by RBS measurement. The relative uncertainty on the concentration value is of 10%.

As seen previously, also in this case the optical absorption analysis does not show any particular feature related to the dopant ions in the matrix. (figure 6.9).

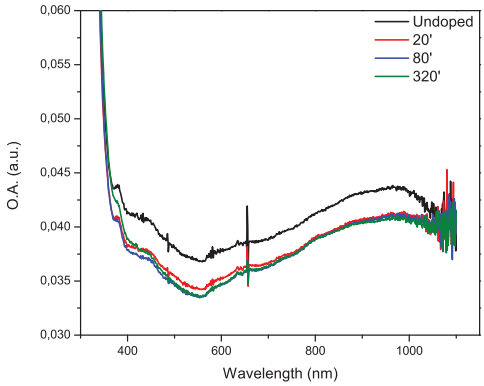

Figure 6.9: Optical absorption spectra of PV cover panels doped by CuCl:NaCl fused bath for different time.

Many information resulted from the luminescence study. Using a wavelength of 260 nm for the excitation, the emission spectrum of the undoped glass is increased in intensity (figure 6.10); recording the excitation spectra at 457 nm and 510 nm (figures 6.11 and 6.12) an increasing of the absorption around 300 nm for the doped glasses is noticeable.

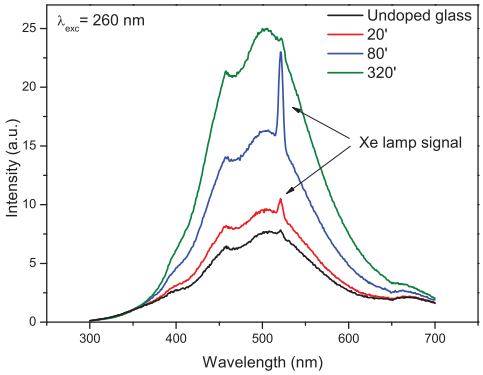

Figure 6.10: Emission spectra of PV cover panels doped by CuCl:NaCl fused bath for different time; $\lambda_{exc.}$= 260 nm. The sharp peak close to $2\lambda_{exc.}$ in the PL spectra is an unfiltered spurious signal due to the Xe lamp.

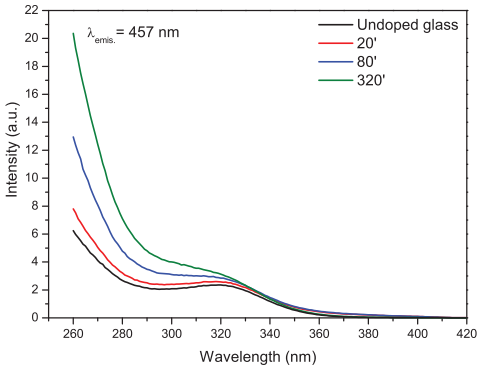

Figure 6.11: Excitation spectra of PV cover panels doped by CuCl:NaCl fused bath for different time; $\lambda_{emis.}$= 457 nm.

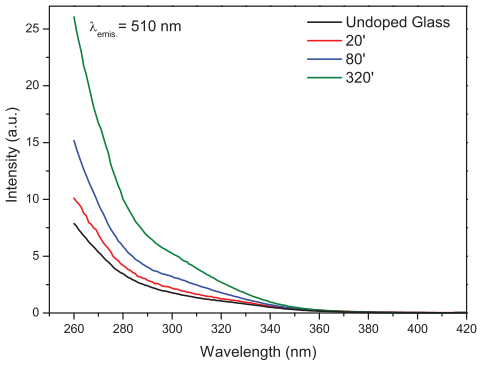

Figure 6.12: Excitation spectra of PV cover panels doped by CuCl:NaCl fused bath for different time; $\lambda_{emis.}$= 510 nm.

Considering the position and the trend of the absorption bands recorded it is possible to associate them to the cuprous ions and as consequence, the increment on the emission spectra to the green emission by Cu^{+} ions. Photoluminescence analysis was done also by using an excitation wavelength of 350 nm but only faint emissions over 600 nm were recorded (orange band) (figure 6.13); on the excitation spectra only a tail of absorption is probably present between 320 and 340 nm (figure 6.14).

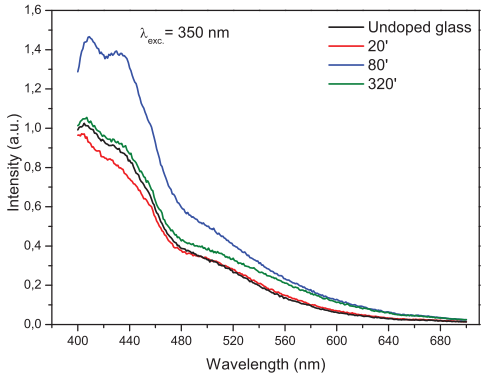

Figure 6.13: Emission spectra of PV cover panels doped by CuCl:NaCl fused bath for different time; $\lambda_{exc.}$= 350 nm.

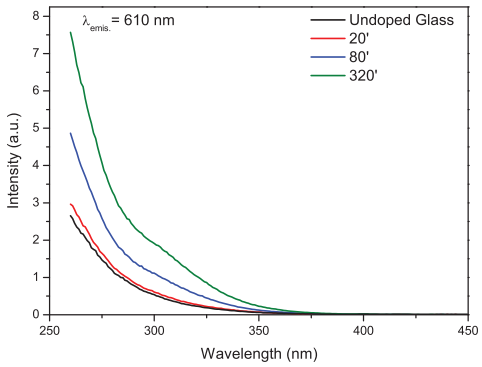

Figure 6.14: Excitation spectra of PV cover panels doped by CuCl:NaCl fused bath for different time; $\lambda_{emis.}$= 610 nm.

6.3 Discussion

The diffusion profiles obtained for samples exchanged by CuZn bath deserve more attention. If a doped glass is maintained at high temperature close to the T_g value without any ion exchange process, it could be expected the dopant atoms will be able to migrate towards the deepest layers inside the matrix, decreasing the initial gradient concentration and the surface concentration too. Comparing the sample exchanged for the shortest time with the longest one, the shape evolution could be explained assuming the glass is not only subjected to the diffusive phenomenon but, being the glass hold at high temperature for a long period of exchange, also a process equivalent to a thermal treatment could be verified. It is like the copper diffusion inside the glass could be active for a period shorter than the total duration of dipping and for the remaining time the temperature could induce the migration of the dopant atoms across the glass; the more is the time of exchange, the more the copper can be spread inside the matrix. In this model the profile observed at 80 minutes of exchange represents a snapshot of the system evolution between 20 minutes and 320 minutes. Is not easy to propose an explanation of why all that occurs. The simulations of RBS profiles were made assuming the ion exchange involves the sodium ions of the glass; probably in case of CuNa bath the presence of Na^+ ions as counter ions inside the bath can have a function on the control of copper migration toward the substrate (competing itself with the TM diffusion). When the glass is dipped inside CuZn bath the diffusion of copper is initially favored due to the absence of sodium ions and the accumulation of copper at the surfaces could be realized. The local high concentration of copper at the interfaces between glass and bath could generate a layer that obstacles the dopant diffusion. At this point being the ulterior diffusion of TM blocked the glass undergoes to a thermal treatment inside the bath. A possible contribute to that is the high Cu^+ concentration ions (probably as consequence of Zn ions) and the more favored diffusion of cuprous ions than cupric ions, being the last ones multivalent.

What results from optical characterization is that after the ion exchange the copper is present as Cu^+ ions and a relatively low presence of copper dimers is ascertained. From the fluorescence analyses of the CuNa series it is resulted that the green emission increases with increasing of the exchange

time and then with the increasing of the copper surface concentration. Actually, the luminescence intensity recorded in case of CuZn bath is comparable with the PL intensity of CuNa bath despite that RBS analysis have shown the highest concentration on dopant atoms in the case of CuNa. A possible explanation could be the quenching effect due to an energy transfer between Cu^{+} ions (donor) and Cu^{2+} ions (acceptor); in general the Cu^{2+} quenching phenomenon is effective only if cupric ions are concentrated over 10^{-3} M. [150]. From the characterization reported before there is not information about the presence of cupric ions inside the samples but some considerations can be done. The RBS analyses of CuNa samples have shown that copper is mainly concentrated in the first layers of the glass and the exchange process involved the Na^{+} ions of the matrix; as a consequence it is possible to assume that along the exchanged layers the concentration of alkaline ions is lower than in the initial glass composition and the optical basicity of the exchanged layers is lower than for the virgin glass.
In general TM ions are assumed to be coordinated in glass as aqua-coordinated ions but being part of the glassy network they are able to feel an alteration on basicity occurred far from the anionic site wherein the ion is placed [166]. Moreover it is well known that the disproportionation reaction is shifted toward the oxidized state if the optical basicity is decreased [36]. Considering that, when copper ions are placed inside the glass by the exchange process, the changes on composition could induce the oxidation of copper from Cu^{+} to Cu^{2+} primarily in the first layers under the surfaces where the dopant concentration is the highest. In this condition it is possible that locally the presence of cupric ions is high enough to realize the quenching of Cu^{+} emission over hypothesized. The general improvement of the emission with the exchange duration underlines that the emissions recorded is the result of two competitive phenomena: the increasing of Cu^{+} concentration and the quenching effect.
A change on optical basicity degree can be used to justify the luminescent trends of the CuZn series. What is resulted is that the sample in which the copper is concentrated under the surfaces (20 minutes of exchange) shows the lowest green band intensity. The evolution of the concentration profile has already been justified as a consequence of a phenomenon similar to a thermal treatment that makes copper ions to migrate inside the matrix but the thermal diffusion can involve also the other mobile ions of the matrix

(Na^+ and K^+), changing the alkali distribution along the glass layers, the optical basicity and then inducing the stabilization of the dopant oxidation state as Cu^+. In other words, after 20 minutes of dipping the first 100 nm in depth are dopant-concentrated and alkali-depleted. For periods of exchange longer than 20 minutes (80 and 320 minutes) the migration of copper and the diffusion of the alkali ions through the matrix cause an average increasing of optical basicity and the dilution of dopant concentration inside the exchanged layers so that the general environment around Cu^+ ions is more useful for its green emission.

Reporting the results in the frame of the down-shifting systems, the main information obtained is that the copper doped cover glasses absorb the light radiations under 350 nm, i.e for whose wavelengths the cell is less active, and emit in the visible range where the PV panel is more efficient. So in principle these systems possess the principal characteristics for acting as LDS. Also the overlap between absorption band and emission has been calculated and reported in the following table (6.1). The calculation of the overlap relative to the orange band (610 nm) is not reported due to the experimental conditions that not allow to calculate it. Considering the glass exchanged for 80 minutes with CuZn bath shows the highest emitted intensity and the lowest overlap it is possible to presume this could be the best performing sample.

Duration	Bath	
	CuZn	CuNa
$20'$	5.2%	1%
$80'$	0.4%	0.8%
$320'$	0.5%	0.5%

Table 6.1: Percentage of overlapping between green emission and absorption band.

6.4 Solar cell power measurements

The output power by the cell covered with glasses doped by CuZn bath is reported in figure 6.15. As it can been seen the samples exchanged for the shortest and the longest time do not improve the yield because the power produced is lower than that of cell covered by the undoped glass. The sample exchanged for 80 minutes shows a little increment of the power produced respect to the virgin cover panel glass; the gain is about 0.8%.

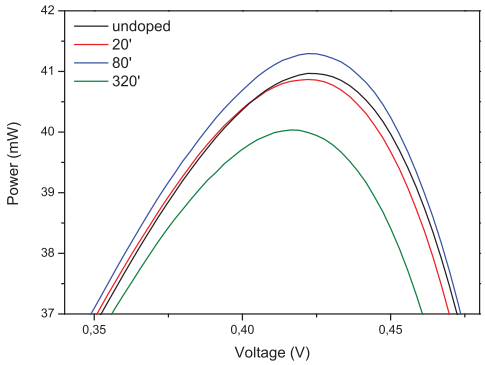

Figure 6.15: Power produced by PV cell covered with the Cu-doped glasses by CuCl:$ZnCl_2$ bath.

Analyzing the sample exchange by CuCl:NaCl bath no improvement of the yield respect the undoped glass is recorded (figure 6.16).

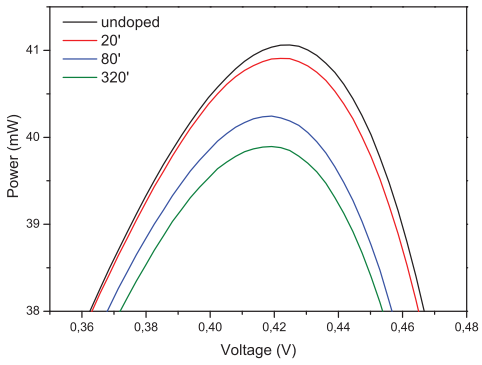

Figure 6.16: Power produced by PV cell covered with Cu-doped glasses by CuNa bath.

6.5 Conclusions

The aim of this work has been to generate down-shifting phenomena by doping the PV cover panel glasses with a transition metal having luminescence properties. The glasses have been doped by ion exchange process with copper ions, exploring two different chloride copper salt mixture for the doping: CuCl:$ZnCl_2$ and CuCl:NaCl. RBS analyses showed a particular evolution of the dopant profile with the increasing of exchange time; being these features observed only for samples exchanged by CuZn bath they have been justified assuming the zinc inside the bath could somehow affect the dopant diffusion. The optical absorption spectra did not give any information about the presence of copper but the photoluminescence spectra let us to record the typical blue-green band generated by the Cu^+ ions in the glass. The trends on the emission band were discussed involving a possible effect of quenching by Cu^{2+} ions as the result of the oxidation of copper ions from 1+ to 2+ state due to a local change on optical basicity degree. The luminescence study showed that the copper doped glasses absorb light between 260 nm and 350 nm and emit photons around 500 nm, showing to posses the basic features to be used in the field of LDS (despite that the PLE and PL spectra are overlapped each other). Finally the samples have been tested with a home-made solar simulator apparatus to obtain a qualitative evaluation on the effective utility of the doped glasses. It has been evidenced that only the sample with the most intense emission and the lowest overlap can induce a slightly improvement of the maximum power produced by the solar cell (below the 1%). This result is coherent with the down-shifting theory but is worth to underline that it could be affected by the quality of the apparatus used for this measurement. For this reason the future developments of this work could be represented by the measurement of EQE and PLQE to prove clearly the copper doped glasses can realize down-shifting phenomena and by recording the XANES spectra to study the copper oxidation state. It could be interesting to analyze the surface quality of the doped glasses for understanding if the ion exchange affects the surfaces too. Moreover, on the basis of the results obtained, changing the optical basicity degree of the glass used could be useful for the control of the copper oxidation state and then for the optimization of the luminescence properties; to do that, glasses of different composition should be studied but as consequence of the

industrial application, the mechanical and structural requirements must be always fulfilled. At last, the cover glass panels are usually chemical tempered and the surfaces are treated by a texturing coating; the influences of these processes on the dopant distribution and on its optical feature must be taken in account and verified.

CHAPTER 7

General conclusions

In this work the ion exchange by molten salt bath has been used to dope silicate glasses with transition metals. In the first part of the thesis, glasses with different optical basicity (OB) degree (0.51, 0.53 and 0.58) have been silver doped to study the relation between the matrix features and the dopant oxidation state. The samples synthesized were mainly analyzed by nuclear (RBS) and optical techniques (optical absorption and fluorescence spectroscopies) that allowed us to obtain information about the concentration and oxidation state of the dopant ions. The optical absorption spectrum collected in case of OB=0.51 (glass with the lowest optical basicity) showed the SPR signal, evidencing the probable formation of nanoparticles during the exchange process. Finally, the silver ions reduction has been justified on the basis of a redox reaction between silver and copper ions. In the case of BK7 glass (OB=0.53) the blue photoemission evidences how the silver is present inside the matrix as Ag^{+} and $Ag^{+}-Ag^{+}$ pairs. Differently for soda-lime glass (OB=0.58) the huge orange emission on the PL spectrum and the absorption tail over 350 nm on optical absorption spectrum have been interpreted as the consequence of the formation of silver structures with oxidation state equal and/or higher than 1+. The results from this preliminary study suggest the increase of the matrix optical basicity promotes the stabilization of the highest oxidation states of a TM also if it is introduced by ion exchange inside hosting medium. This outcome is in agreement with the

knowledge about the relation between optical basicity and oxidation state of TMs studied by melt quenching technique. The second part of the thesis has been mainly devoted to the realization of down-shifting phenomena inside the cover glass of the photovoltaic panels, with the aim at increasing the solar cell output power. To do that, the doping of PV panels with silver or copper were studied due to the interesting optical features of these two TMs. Silver doped glasses did not increase the power produced by the solar cell; that was justified on the base of the silver aggregates formation that increases the UV-VIS absorption of the doped glasses. To avoid this problem, the right post doping annealing condition must be determined to enhance the formation of emitting silver aggregates and at the same time, to reduce the UV-VIS absorption. In literature, the existence of a threshold temperature for the formation of high absorbing clusters is predicted. Soda-lime glasses were then doped with silver by dipping inside $AgNO_3$:$NaNO_3$ bath at 320 °C for 1h. After the doping the sample were thermal annealed in air at 380 °C, 410 °C and 440 °C; the durations of 1 h, 4 h and 16 hours were investigated. The sample with the best balance between absorption and emission features appears to be the glass treated at 410 °C for 16 hours. Nevertheless, with this glass used as cover an increment of the PV output power has not been evidenced. From the first attempts about the use of copper for the doping, it resulted that only the PV panels doped with copper by dipping in CuCl:$ZnCl_2$ eutectic mixture are able to increase the maximum power produced by the cell. This has been justified by the control, on these samples, of the quenching effect of the Cu^+ green emission by Cu^{2+} ions. By XANES analyses the fraction of Cu^{2+} ions has been determined. Having the glass exchanged at 400 °C for 4 h the less presence of cupric ions and the highest green emission intensity, it has been chosen to investigate more deeply this temperature. To do that, PV cover glass panels were doped by dipping inside CuCl:$ZnCl_2$ fused bath at the temperature of 400 °C for 20, 80 and 320 minutes; moreover the same was done by using a CuCl:NaCl eutectic molten bath. The copper doped glasses resulted uncolored and they showed to absorb light around 350 nm and to emit around 510 nm; moreover, the absorption and emission bands resulted overlapped. The luminescence trends were justified invoking the quenching effect of Cu^+ emission band (510 nm) by Cu^{2+} ions. The oxidation of copper ions has been interpreted on the basis of the optical basicity change along the exchanged glass layers

as the consequence of the alkali ions migration during the doping process. The exchanged glasses were tested as PV cover panel: only the sample with the highest emission intensity and the lowest overlap between absorption and emission bands was able to improve the yield of the solar cell. At this point some developments can be suggested. About the first topic, namely the relation between optical basicity and oxidation state, it could be interesting to do a systematical study of the TM oxidation state inside glasses of different OB. For example, by taking advantage by the sol-gel synthesis it could be possible to synthesize glass layers with a large variety of optical basicity degree, thus doping them with TM by ion exchange and studying the oxidation state. About the down-shifting, first of all it is important to complete the characterization of the most promising samples with the measurement of the external quantum efficiency (EQE) to verify the effectiveness of the down-shifting phenomenon. After that, the work could be driven toward the research of the best synthesis condition for the improvement of the doped glasses PLQY. In particular, referring to silver doped glasses, it is fundamental to go further in the research of the best post annealing conditions. In this frame the conditions suggested by the statistical simulation of the emission intensity must be verified. In general, an analysis able to determine in which way the glass matrix (by the structural and electronic defects) influences the TM doping oxidation state could help to throw light on the whole oxo-reduction equilibria involving the doping elements: in this frame, an experimental approach based on μ–Raman measurements performed in cross-section along the doping depth profile could give findings about the importance of the matrix modifications on the determination of the final chemical state of the doping TM: this is one of the possible next approach about the basic aspects of the research here reported.

Bibliography

[1] F. Gonella and P. Mazzoldi. *Metal Nanocluster Composite Glasses*. Ed. by H. S. Nalwa. Vol. 4. Academic Press, 2000, pp. 81–158.

[2] A. Quaranta, E. Cattaruzza, and F. Gonella. In: *Materials Science and Engineering: B* 149.2 (Mar. 2008), pp. 133–139.

[3] A. Y. Zhang, T. Suetsugu, and K. Kadono. In: *Journal of Non-Crystalline Solids* 353.1 (Jan. 2007), pp. 44–50.

[4] T. Pradell, J. Molera, J. Roque, M. Vendrell-Saz, A. D. Smith, E. Pantos, and D. Crespo. In: *Journal of the American Ceramic Society* 88.5 (May 2005), pp. 1281–1289.

[5] P. Mazzoldi and C. Sada. In: *Materials Science and Engineering: B* 149.2 (Mar. 2008), pp. 112–117.

[6] G. Schulze. In: *Annalen der Physik* 345.2 (1913), pp. 335–367.

[7] S. S. Kistler. In: *Journal of the American Ceramic Society* 45.2 (Feb. 1962), pp. 59–68.

[8] M. E. Nordberg, E. L. Mochel, H. M. Garfinkel, and S. J. Olcott. In: *Journal of the American Ceramic Society* 47.5 (Feb. 1962), pp. 215–219.

[9] A. K. Varshneya. In: *International Journal of Applied Glass Science* 1.2 (Mar. 2010), pp. 131–142.

[10] J. E. Goell and R. D. Standley. In: *Proceedings of the IEEE* 58.10 (Oct. 1970), pp. 1504–1512.

[11] C. Sada, E. Borsella, F. Caccavale, F. Gonella, F. Segato, Y. N. Korkishko, V. A. Fedorov, T. M. Morozova, G. Battaglin, and R. Polloni. In: *Applied Physics Letters* 72.26 (June 1998), pp. 3431–3433.

[12] J. L. Jackel. In: *Applied Physics Letters* 41.7 (1982), pp. 607–608.

[13] A. Quaranta, S. Carturan, M. Bonafini, G. Maggioni, M. Tonezzer, G. Mattei, C. de Julián Fernandez, G. Della Mea, and P. Mazzoldi. In: *Sensors and Actuators B: Chemical* 118.1–2 (2006), pp. 418–424.

[14] C. Maurzio, F. D'Acapito, E. Ghibaudo, and J. E. Broquin. In: *Journal of Non-Crystalline Solids* 354.2-9 (Jan. 2008), pp. 124–128.

[15] A. Beguin, T. Dumas, M. J. Hackert, R. Jansen, and C. Nissim. In: *Journal of Lightwave Technology* 6.10 (Oct. 1988), pp. 1483–1487.

[16] G. H. Chartier, P. Jaussaud, A. D. de Oliveira, and O. Parriaux. In: *Electronics Letters* 13.25 (Dec. 1977), pp. 763–764.

[17] V. Neuman, O. Parriaux, and L. M. Walpita. In: *Electronics Letters* 15.22 (Oct. 1979), pp. 704–706.

[18] A. Mackova, V. Perina, V. Havranek, P. Tresnakova-Nebolova, J. Spirkova, and O. Telezhnikova. In: *Surface Science* 566-568 (Sept. 2004), pp. 111–114.

[19] L. Salavcova, J. Spirkova, M. Mika, A. Mackova, J. Oswald, A. Langrova, and J. Vacik. In: *Optical Materials* 29.7 (Mar. 2007), pp. 753–759.

[20] A. Mackova, V. Havranek, J. Vacik, L. Salavcova, and J. Spirkova. In: *Nuclear Instruments and Methods in Physics Research Section B: Beam Interactions with Materials and Atoms* 249.1-2 (Aug. 2006), pp. 856–858.

[21] L. Salavcova, A. Mackova, J. Oswald, B. Svecova, S. Janakova, J. Spirkova, and M. Mika. In: *Journal of Physics and Chemistry of Solids* 68.5-6 (May 2007), pp. 891–895.

[22] J. J. Torres-Castañon, A. V. Gorokhovskii, V. A. Zhabrev, A. F. Fuentes, J. I. Escalante-Garcia, and E. V. German. In: *Glass Physics and Chemistry* 30.2 (Mar. 2004), pp. 167–172.

[23] J. L. Jackel. In: *Applied Optics* 27.3 (Feb. 1988), pp. 472–475.

[24] T. Izawa and H. Nakagome. In: *Applied Physics Letters* 21.12 (1972), pp. 584–586.

[25] E. Cattaruzza, G. Battaglin, F. Gonella, S. Ali, C. Sada, and A. Quaranta. In: *Materials Science and Engineering: B* 149.2 (Mar. 2008), pp. 195–199.

[26] H. Flood, T. Forland, and K. Motzfeldt. In: *Acta Chemica Scandinavica* 6 (1952), pp. 257–269.

[27] J. A. Duffy and M. D. Ingram. In: *Journal of the American Chemical Society* 93.24 (Dec. 1971), pp. 6448–6454.

[28] G. Ottonello and R. Moretti. In: *Journal of Physics and Chemistry of Solids* 65.8-9 (Aug. 2004), pp. 1609–1614.

[29] J. A. Duffy. In: *Journal of Chemical Education* 73.12 (Dec. 1996), pp. 1138–1142.

[30] J. A. Duffy and F. G. K. Baucke. In: *The Journal of Physical Chemistry* 99.22 (June 1995), pp. 9189–9193.

[31] J. A. Duffy. In: *Journal of Non-Crystalline Solids* 86.1-2 (Sept. 1986), pp. 149–160.

[32] D. R. Gaskell. In: *Transactions of the Iron and Steel Institute of Japan* 22.12 (1982), pp. 997–1000.

[33] J. A. Duffy. In: *Geochimica et Cosmochimica Acta* 57.16 (Aug. 1993), pp. 3961–3970.

[34] A. Terczynska-Madej, K. Cholewa-Kowalska, and M. Laczka. In: *Optical Materials* 32.11 (Sept. 2010), pp. 1456–1462.

[35] J. A. Duffy. In: *Journal of Non-Crystalline Solids* 196.95 (Mar. 1996), pp. 45–50.

[36] J. Kaufmann and C. Rüssel. In: *Journal of Non-Crystalline Solids* 354.40-41 (Oct. 2008), pp. 4614–4619.

[37] W. Thiemsorn, K. Keowkamnerd, S. Phanichphant, P. Suwannathada, and H. Hessenkemper. In: *Glass Physics and Chemistry* 34.1 (Jan. 2011), pp. 19–29.

[38] B. Svecova, J. Spirkova, S. Janakova, and M. Mika. In: *Materials Science and Engineering: B* 149.2 (Mar. 2008), pp. 177–180.

[39] P. Capek, M. Mika, J. Oswald, P. Tresnakova, L. Salavcova, O. Kolek, J. Schrofel, and J. Spirkova. In: *Optical Materials* 27.2 (Nov. 2004), pp. 331–336.

[40] P. C. Schultz. In: *Journal of the American Ceramic Society* 57.7 (July 1974), pp. 309–313.

[41] J. Qiu, M. Shirai, T. Nakaya, J. Si, X. Jiang, C. Zhu, and K. Hirao. In: *Applied Physics Letters* 81.16 (2002), pp. 3040–3042.

[42] A. Nahal and K. Shapoori. In: *Applied Surface Science* 255.18 (June 2009), pp. 7946–7950.

[43] U. Kreibig and M. Vollmer. In: *Optical Properties of Metal Clusters* (1995).

[44] B. Ghosh, P. Chakraborty, S. Mohapatra, P. A. Kurian, C. Vijayan, P.C. Deshmukh, and P. Mazzoldi. In: *Materials Letters* 61.23-24 (Sept. 2007), pp. 4512–4515.

[45] D. Manikandan, S. Mohan, P. Magudapathy, and K. G. M. Nair. In: *Physica B: Condensed Matter* 325 (Jan. 2003), pp. 86–91.

[46] R. H. Magruder, J. E. Wittig, and R. A. Zuhr. In: *Journal of Non-Crystalline Solids* 163.2 (Nov. 1993), pp. 162–168.

[47] Y. H. Wang, S. J. Peng, J. D. Lu, R. W. Wang, Y. L. Mao, and Y. G. Cheng. In: *Vacuum* 83.2 (Sept. 2008), pp. 408–411.

[48] M. Valodkar, S. Modi, A. Pal, and S. Thakore. In: *Materials Research Bulletin* 46.3 (Mar. 2011), pp. 384–389.

[49] S. Chowdhury, V. R. Bhethanabotla, and R. Sen. In: *The Journal of Physical Chemistry C* 113.30 (July 2009), pp. 13016–13022.

[50] C. Noguez. In: *The Journal of Physical Chemistry C* 111.10 (Mar. 2007), pp. 3806–3819.

[51] P. K. Jain and M. A. El-Sayed. In: *The Journal of Physical Chemistry C* 111.47 (Nov. 2007), pp. 17451–17454.

[52] K. L. Kelly, E. Coronado, L. L. Zhao, and G. C. Schatz. In: *The Journal of Physical Chemistry B* 107.3 (Jan. 2003), pp. 668–677.

[53] A. Simo, J. Polte, N. Pfänder, U. Vainio, F. Emmerling, and K. Rademann. In: *Journal of the American Chemical Society* 134.45 (Nov. 2012), pp. 18824–18833.

[54] E. Borsella, F. Gonella, P. Mazzoldi, A. Quaranta, G. Battaglin, and R. Polloni. In: *Chemical Physics Letters* 284.5-6 (Mar. 1998), pp. 429–434.

[55] E. Borsella, G. Battaglin, M. A. García, F. Gonella, P. Mazzoldi, R. Polloni, and A. Quaranta. In: *Applied Physics A: Materials Science & Processing* 71.2 (2000), pp. 125–132.

[56] G. Medhi, P. Nandi, S. Mohan, and G. Jose. In: *Materials Letters* 61.11-12 (May 2007), pp. 2259–2261.

[57] A. V. Podlipensky, V. Grebenev, G. Seifert, and H. Graener. In: *Journal of Luminescence* 109.3-4 (Sept. 2004), pp. 135–142.

[58] E. Borsella, E. Cattaruzza, G. De Marchi, F. Gonella, G. Mattei, P. Mazzoldi, A. Quaranta, G. Battaglin, and R. Polloni. In: *Journal of Non-Crystalline Solids* 245.1-3 (Apr. 1999), pp. 122–128.

[59] P. Boutinaud, E. Duloisy, C. Pedrini, B. Moine, C. Parent, and G. Le Flem. In: *Journal of Solid State Chemistry* 94.2 (Oct. 1991), pp. 236–243.

[60] J. A. Duffy and M. D. Ingram. In: *Comptes Rendus Chimie* 5.11 (Nov. 2002), pp. 797–804.

[61] V. Dimitrov and T. Komatsu. In: *Journal of Solid State Chemistry* 196 (Dec. 2012), pp. 574–578.

[62] J. A. Duffy. In: *Physics and Chemistry of Glasses* 40.2 (1999), pp. 54–56.

[63] A. Rahman, M. Giarola, E. Cattaruzza, F. Gonella, M. Mardegan, E. Trave, A. Quaranta, and G. Mariotto. In: *Journal of Nanoscience and Nanotechnology* 12.11 (Nov. 2012), pp. 8573–8579.

[64] M. Eichelbaum, K. Rademann, A. Hoell, D. M. Tatchev, W. Weigel, R. Stöß er, and G. Pacchioni. In: *Nanotechnology* 19.13 (Apr. 2008), pp. 135701–135710.

[65] S. Takeda, K. Yamamoto, and M. Matsumoto. In: *Journal of Non-Crystalline Solids* 265.1-2 (Mar. 2000), pp. 133–142.

[66] S. Takeda, R. Akiyama, and H. Hosono. In: *Journal of Non-Crystalline Solids* 311.3 (Dec. 2002), pp. 273–280.

[67] R. A. Weeks. In: *Journal of Non-Crystalline Solids* 179.4 (Nov. 1994), pp. 1–9.

[68] L. Zhang, V. Mashkov, and R. Leisure. In: *Physical Review Letters* 74.9 (Feb. 1995), pp. 1605–1608.

[69] K. Kajihara, L. Skuja, M. Hirano, and H. Hosono. In: *Physical Review Letters* 92.1 (Jan. 2004), pp. 15504–15508.

[70] A. Edwards and W. Fowler. In: *Physical Review B* 26.12 (Dec. 1982), pp. 6649–6660.

[71] L. Jiang and J. Sheng. In: *Journal of Materials Science* 40.19 (Oct. 2005), pp. 5177–5180.

[72] J. Sheng, X. Yang, W. Dong, and J. Zhang. In: *International Journal of Hydrogen Energy* 34.9 (May 2009), pp. 3988–3991.

[73] P. Ebeling, D. Ehrt, and M. Friedrich. In: *Optical Materials* 20.2 (Sept. 2002), pp. 101–111.

[74] A. Bishay. In: *Journal of Non-Crystalline Solids* 3.1 (Jan. 1970), pp. 54–114.

[75] D. L. Griscom and M. Mizuguchi. In: *Journal of Non-Crystalline Solids* 239.1-3 (Oct. 1998), pp. 66–77.

[76] A. Quaranta, A. Rahman, G. Mariotto, C. Maurizio, E. Trave, F. Gonella, E. Cattaruzza, E. Gibaudo, and J. E. Broquin. In: *The Journal of Physical Chemistry C* 116.5 (Feb. 2012), pp. 3757–3764.

[77] D. W. Matson, S. K. Sharma, and J. A. Philpotts. In: *Journal of Non-Crystalline Solids* 58.2-3 (Nov. 1983), pp. 323–352.

[78] P. McMillan. In: *American Mineralogist* 69 (1984), pp. 622–644.

[79] H. D. Schreiber, G. B. Balazs, B. E. Carpenter, J. E. Kirkley, L. M. Minnix, P. L. Jamison, and T. O. Mason. In: *Journal of the American Ceramic Society* 67.6 (June 1984), pp. 106–108.

[80] H. D. Schreiber, N. R. Wilk Jr, and C. W. Schreiber. In: *Journal of Non-Crystalline Solids* 253.1-3 (Aug. 1999), pp. 68–75.

[81] O. Clauß en and C. Rüssel. In: *Berichte der Bunsengesellschaft für physikalische Chemie* 100.9 (Sept. 1996), pp. 1475–1478.

[82] H. D. Schreiber and M. Todd Coolbaugh. In: *Journal of Non-Crystalline Solids* 181.3 (Feb. 1995), pp. 225–230.

[83] J. Sheng, J. Li, and J. Yu. In: *International Journal of Hydrogen Energy* 32.13 (Sept. 2007), pp. 2598–2601.

[84] J.-P. Blondeau, S. Pellerin, V. Vial, K. Dzierżega, N. Pellerin, and C. Andreazza-Vignolle. In: *Journal of Crystal Growth* 311.1 (Dec. 2008), pp. 172–184.

[85] G. W. Arnold, G. De Marchi, F. Gonella, P. Mazzoldi, A. Quaranta, G. Battaglin, M. Catalano, F. Garrido, and R. F. Haglund. In: *Nuclear Instruments and Methods in Physics Research Section B: Beam Interactions with Materials and Atoms* 116.1-4 (Aug. 1996), pp. 507–510.

[86] E. Cattaruzza, M. Mardegan, E. Trave, G. Battaglin, P. Calvelli, F. Enrichi, and F. Gonella. In: *Applied Surface Science* 257.12 (Apr. 2011), pp. 5434–5438.

[87] S. A. Gamboa, H. Nguyen-Cong, P. Chartier, P. J. Sebastian, M. E. Calixto, and M. A. Rivera. In: *Solar Energy Materials and Solar Cells* 55.1-2 (July 1998), pp. 95–104.

[88] G. Gordillo and C. Calderón. In: *Solar Energy Materials and Solar Cells* 77.2 (May 2003), pp. 163–173.

[89] F. H. Karg. In: *Solar Energy Materials and Solar Cells* 66.1-4 (Feb. 2001), pp. 645–653.

[90] T. Negami, Y. Hashimoto, and S. Nishiwaki. In: *Solar Energy Materials and Solar Cells* 67.1-4 (Mar. 2001), pp. 331–335.

[91] T. Nakada, M. Mizutani, Y. Hagiwara, and A. Kunioka. In: *Solar Energy Materials and Solar Cells* 67.1-4 (Mar. 2001), pp. 255–260.

[92] J. C. C. Fan, C. O. Bozler, and R. W. McClelland. In: *15th Photovoltaic Specialists Conference*. 1981, pp. 666–672.

[93] K. L. Chopra, P. D. Paulson, and V. Dutta. In: *Progress in Photovoltaics: Research and Applications* 12.23 (Mar. 2004), pp. 69–92.

[94] E. Klampaftis, D. Ross, K. R. McIntosh, and B. S. Richards. In: *Solar Energy Materials and Solar Cells* 93.8 (Aug. 2009), pp. 1182–1194.

[95] E. Barlow, N. Billimoria, and R. Fernandez. In: *Materials Science and Engineering* ().

[96] W. Shockley and H. J. Queisser. In: *Journal of Applied Physics* 32.3 (1961), pp. 510–519.

[97] M. A. Green, K. Emery, Y. Hishikawa, W. Warta, and E. D. Dunlop. In: *Progress in Photovoltaics: Research and Applications* 20 (2012), pp. 12–20.

[98] F. Dimroth and S. Kurtz. In: *MRS Bulletin* 32.03 (2007), pp. 230–235.

[99] M. A. Green and S. R. Wenham. In: *Applied Physics Letters* 65.23 (1994), pp. 2907–2907.

[100] A. J. Heeger. In: *Chemical Society reviews* 39.7 (July 2010), pp. 2354–2371.

[101] A. Luque and A. Martí. In: *Physical Review Letters* 78.26 (June 1997), pp. 5014–5017.

[102] J. Li, M. Chong, J. Zhu, Y. Li, J. Xu, P. Wang, Z. Shang, Z. Yang, R. Zhu, and X. Cao. In: *Applied Physics Letters* 60 (1992), pp. 2240–2242.

[103] P. Brown and P. V. Kamat. In: *Journal of the American Chemical Society* 130.28 (July 2008), pp. 8890–8891.

[104] W. A. Badawy. In: *AIP Conference Proceedings* 888.1 (2007), pp. 29–35.

[105] P. Vitanov, M. Kamenova, N. Tyutyundzhiev, M. Delibasheva, E. Goranova, and M. Peneva. In: *Thin Solid Films* 297.1-2 (Apr. 1997), pp. 299–303.

[106] V. Y. Yerokhov and I. I. Melnyk. In: *Renewable and Sustainable Energy Reviews* 3.4 (Dec. 1999), pp. 291–322.

[107] A. Goetzberger and W. Greube. In: *Applied Physics* 14.2 (Oct. 1977), pp. 123–139.

[108] H. J. Hovel, R. T. Hodgson, and J. M. Woodall. In: *Solar Energy Materials* 2.1 (Sept. 1979), pp. 19–29.

[109] S. Marchionna, F. Meinardi, M. Acciarri, S. Binetti, A. Papagni, S. Pizzini, V. Malatesta, and R. Tubino. In: *Journal of Luminescence* 118.2 (June 2006), pp. 325–329.

[110] T. Maruyama, A. Enomoto, and K. Shirasawa. In: *Solar Energy Materials and Solar Cells* 64.3 (Oct. 2000), pp. 269–278.

[111] B. S. Richards and K. R. McIntosh. In: *Progress in Photovoltaics: Research and Applications* 15.1 (Jan. 2007), pp. 27–34.

[112] G. Wang, Q. Peng, and Y. Li. In: *Journal of the American Chemical Society* 131.40 (Oct. 2009), pp. 14200–14201.

[113] X. Huang, S. Han, W. Huang, and X. Liu. In: *Chemical Society Reviews* 42.1 (2013), pp. 173–201.

[114] Y. Jestin. In: *Comprehensive Renewable Energy* 1 (2012), pp. 563–586.

[115] Y. Jestin, G. Pucker, M. Ghulinyan, L. Ferrario, P. Bellutti, A. Picciotto, A. Collini, A. Marconi, A. Anopchenko, Z. Yuan, and L. Pavesi. In: *Proc. SPIE* 7772 (2010), pp. 77720–77727.

[116] V. Švrček, A. Slaoui, and J. C. Muller. In: *Thin Solid Films* 451-452 (Mar. 2004), pp. 384–388.

[117] W. G. J. H. M. van Sark. In: *Applied Physics Letters* 87.15 (2005), pp. 151117–151120.

[118] A. N. Nazarov, S. I. Tiagulskyi, I. P. Tyagulskyy, V. S. Lysenko, L. Rebohle, J. Lehmann, S. Prucnal, M. Voelskow, and W. Skorupa. In: *Journal of Applied Physics* 107.12 (2010), p. 123112.

[119] W. Wu, T. Wang, X. Wang, S. Wu, Y. Luo, X. Tian, and Q. Zhang. In: *Solar Energy* 84.12 (Dec. 2010), pp. 2140–2145.

[120] T. Wang, J. Zhang, W. Ma, Y. Luo, L. Wang, Z. Hu, W. Wu, X. Wang, G. Zou, and Q. Zhang. In: *Solar Energy* 85.11 (Nov. 2011), pp. 2571–2579.

[121] J. Graffion, X. Cattoën, M. Wong Chi Man, V. R. Fernandes, P. S. André, R. A. S. Ferreira, and L. D. Carlos. In: *Journal of Materials Chemistry* 23.21 (2011), pp. 4773–4782.

[122] A. Le Donne, M. Acciarri, D. Narducci, S. Marchionna, and S. Binetti. In: *Progress in Photovoltaics: Research and Applications* 17.8 (2009), pp. 519–525.

[123] Z. Cheng, L. Pan, F. Su, M. Cao, and Z. Sun. In: *Surface Review and Letters* 16.05 (2009), pp. 669–673.

[124] B. C. Hong and K. Kawano. In: *Solar Energy Materials and Solar Cells* 80.4 (Dec. 2003), pp. 417–432.

[125] T. Jin, S. Inoue, K. Machida, and G. Adachi. In: *Journal of The Electrochemical Society* 144.11 (1997), pp. 4054–4058.

[126] K. Kawano, N. Hashimoto, and R. Nakata. In: *Materials Science Forum*. Vol. 239-241. 1997, pp. 311–314.

[127] A. F. Mansour. In: *Polymer Testing* 22.5 (Aug. 2003), pp. 491–495.

[128] K. McIntosh and B. Richards. In: *2006 IEEE 4th World Conference on Photovoltaic Energy Conference*. Vol. 2. IEEE, May 2006, pp. 2108–2111.

[129] L. H. Slooff, R. Kinderman, A. R. Burgers, N. J. Bakker, J. A. M. van Roosmalen, A. Buchtemann, R. Danz, and M. Schleusener. In: *Journal of Solar Energy Engineering* 129.3 (2007), pp. 272–276.

[130] K. R. McIntosh, G. Lau, J. N. Cotsell, K. Hanton, D. L. Bätzner, F. Bettiol, and B. S. Richards. In: *Progress in Photovoltaics: Research and Applications* 17.3 (2009), pp. 191–197.

[131] R. A. Zakhidov and A. I. Koifman. In: *Applied Solar Energy* 30.4 (1994), pp. 22–25.

[132] S. Gómez, I. Urra, R. Valiente, and F. Rodríguez. In: *Solar Energy Materials and Solar Cells* 95.8 (Aug. 2011), pp. 2018–2022.

[133] L. A. B. Pilkington. In: *Proceedings Of The Royal Society of London A. Mathematical And Physical Sciences* 314.1516 (1969), pp. 1–25.

[134] Y. Hayashi, Y. Fukuda, and M. Kudo. In: *Surface Science* 507-510 (June 2002), pp. 872–876.

[135] S. Takeda. In: *Journal of Non-Crystalline Solids* 352.36-37 (Oct. 2006), pp. 3910–3913.

[136] Q. Zhang, Z. Chen, and Z. Li. In: *Science China Technological Sciences* 54.3 (Jan. 2011), pp. 691–697.

[137] M. Dimitrova, Y. Ivanova, and Y. Dimitriev. In: *Journal of the University of Chemical Technology and Metallurgy* 47.4 (2012), pp. 409–414.

[138] Y. Dimitriev, Y. Ivanova, A. El D. T. Aly, M. Gancheva, and R. Iordanova. In: *Journal of the University of Chemical Technology and Metallurgy* 47.4 (2012), pp. 415–420.

[139] H. Márquez, D. Salazar, A. Villalobos, G. Paez, and J. Ma. Rincón. In: *Applied Optics* 34.25 (Sept. 1995), pp. 5817–5822.

[140] D. Salazar, H. Porte, and H. Márquez. In: *Applied Optics* 36.34 (Dec. 1997), pp. 8987–8991.

[141] B. Macalik, L. Krajczyk, J. Okal, T. Morawska-Kowal, K. D. Nierzewski, and M. Suszyńska. In: *Radiation Effects and Defects in Solids* 157.6-12 (2002), pp. 887–893.

[142] J. F. Pérez-Robles, F. J. Garcıa-Rodrıguez, J. M. Yáñez Limón, F. J. Espinoza-Beltrán, Y. V. Vorobiev, and J. González-Hernández. In: *Journal of Physics and Chemistry of Solids* 60.10 (Oct. 1999), pp. 1729–1736.

[143] M. Zhao, L. Sun, and R. M. Crooks. In: *Journal of America Chemical Society* 7863.21 (1998), pp. 4877–4878.

[144] A. Quaranta, R. Ceccato, C. Menato, L. Pederiva, N. Capra, and R. Dal Maschio. In: *Journal of Non-Crystalline Solids* 345-346 (Oct. 2004), pp. 671–675.

[145] M. A. Garcıía, E. Borsella, S. E. Paje, J. Llopis, M. A. Villegas, and R. Polloni. In: *Journal of Luminescence* 93.3 (July 2001), pp. 253–259.

[146] R. Debnath. In: *Journal of Luminescence* 43.6 (Aug. 1989), pp. 375–377.

[147] R. Debnath and S. K. Das. In: *Chemical Physics Letters* 155.1 (Feb. 1989), pp. 52–58.

[148] R. Debnath and S. Kumar. In: *Journal of Non-Crystalline Solids* 123.1-3 (Aug. 1990), pp. 271–274.

[149] Y. Ti, F. Qiu, Y. Cao, L. Jia, W. Qin, J. Zheng, and G. Farrell. In: *Journal of Materials Science* 43.22 (Oct. 2008), pp. 7073–7078.

[150] Y. Fujimoto and M. Nakatsuka. In: *Journal of Luminescence* 75.3 (Oct. 1997), pp. 213–219.

[151] T. Lutz, C. Estournès, J. C. Merle, and J. L. Guille. In: *Journal of Alloys and Compounds* 262-263 (Nov. 1997), pp. 438–442.

[152] P. Boutinaud, D. Garcia, C. Parent, M. Faucher, and G. Le Flem. In: *Journal of Physics and Chemistry of Solids* 56.9 (Sept. 1995), pp. 1147–1154.

[153] E. Fargin, I. Bussereau, G. Le Flem, R. Olazcuaga, C. Cartier, and H. Dexpert. In: *European Journal of Solid State and Inorganic Chemistry* 29 (1992), pp. 975–980.

[154] M. Quinten. In: *Zeitschrift für Physik B Condensed Matter* 101.2 (Feb. 2014), pp. 211–217.

[155] P. Nebolova, J. Spirkova, V. Perina, I. Jirka, K. Mach, and G. Kuncova. In: *Solid State Ionics* 141-142 (May 2001), pp. 609–615.

[156] J. Lee, T. Yano, S. Shibata, A. Nukui, and M. Yamane. In: *Journal of Non-Crystalline Solids* 277.2-3 (Nov. 2000), pp. 155–161.

[157] F. Gonella, A. Quaranta, S. Padovani, C. Sada, F. D'Acapito, C. Maurizio, G. Battaglin, and E. Cattaruzza. In: *Applied Physics A* 81.5 (July 2005), pp. 1065–1071.

[158] C. Maurizio, F. D'Acapito, M. Benfatto, S. Mobilio, E. Cattaruzza, and F. Gonella. In: *The European Physical Journal B* 14.2 (Mar. 2000), pp. 211–216.

[159] E. Borsella, A. Dal Vecchio, M. A. Garcıa, C. Sada, F. Gonella, R. Polloni, A. Quaranta, and L. J. G. W. van Wilderen. In: *Journal of Applied Physics* 91.1 (2002), pp. 90–98.

[160] M. Treguer, F. Rocco, G. Lelong, A. Le Nestour, T. Cardinal, A. Maali, and B. Lounis. In: *Solid State Sciences* 7.7 (July 2005), pp. 812–818.

[161] J. Solé, L. Bausa, and D. Jaque. *An Introduction to the Optical Spectroscopy of Inorganic Solids*. John Wiley & Sons, 2005.

[162] P. Atkins and J. De Paola. *Physical Chemistry*. W. H. Freeman and Company, 2009.

[163] D. L. Dexter and J. H. Schulman. In: *The Journal of Chemical Physics* 22.6 (1954), pp. 1063–1070.

[164] R. F. Chen and J. R. Knutson. In: *Analytical Biochemistry* 172.1 (July 1988), pp. 61–77.

[165] D. Peak, T. C. Werner, R. M. Dennin, and J. K. Baird. In: *The Journal of Chemical Physics* 79.7 (1983), pp. 3328–3335.

[166] J. A. Duffy, M. D. Ingram, and S. Fong. In: *Physical Chemistry Chemical Physics* 2.8 (2000), pp. 1829–1833.

[167] Wikipedia. *Theory of solar cells — Wikipedia*.

[168] A. Luque and S. Hegedus. *Handbook of Photovoltaic Science and Engineering*. John Wiley & Sons, 2011.

Appendix A

An introduction to the solar cell.

A solar cell is a device able to convert the photons energy into electrical energy. Nowadays the solar cell technology is founded upon the semiconductor materials in fact the most common solar cells are made by a p-n junction based on the silicon that is one of the most known semiconductor element. When a photon impinges on silicon sheet, if the photon energy is higher than the silicon band gap (1.12 eV) it can be absorbed; as a consequence of that a transition of an electron from the valence band to the conduction band occurs, a positive hole is generated in the valence band obtaining the formation of a mobile electron-hole couple (p-n junction). A p-n junction or diode is a semiconductor that it has been functionalized in such a way to improve the number of electrons produced by the n-type side and the number of holes by the opposite side (p-type side). At the conjunction between p and n side the diffusion of the holes and electrons occurs driven by the gradient concentration; the charges motion induces the formation of a portion of volume (space charged region) where the neutrality of charge is not maintained and, as a consequence of that, an electric field is generated stopping the diffusion of electrons and holes across the space charged region. In this situation if the n-type side and the p-type side are linked each other by a wire, a current starts flowing throughout the conductor.
The solar cell can be described by an equivalent circuit composed by a diode in parallel linked to a source of current (for an ideal solar cell). In the case of a real solar cell the equivalent circuit is more complicated and a shunt resistance (R_{SH} [Ω]) and a series resistance (R_S [Ω]) are needed to be added

(figure 7.1).

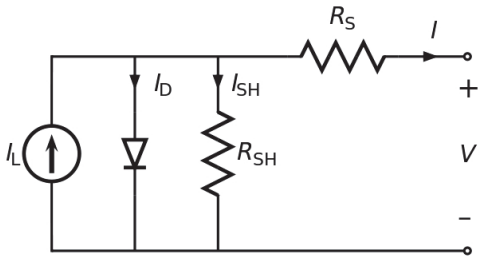

Figure 7.1: Equivalent circuit for a real solar cell where: I is the output current [A]; I_D is the diode current [A]; I_{SH} is the shunt current [A]; I_L is the photogenerated current [A] [167].

Considering that, it is possible to show that the characteristic cell equation is [168]

$$I = I_{SC} - I_0\left[\exp\left(q\frac{(V+IR_S)}{AK_BT}\right)-1\right]-\frac{(V+IR_S)}{R_{SH}} \tag{7.1}$$

where: A is the ideality factor for the cell; T absolute temperature [K]; K_B the Boltzmann's constant; q the elementary charge [C]. Being the equation 7.1 a transcendental function it is solved by numerical methods.
The cell behavior can be evaluated by the measurement of the power produced by the photovoltaic cell and that is possible to be done collecting the I vs V curve of the cell placed under a constant illumination and at fixed temperature. The I-V sweep lets us to evaluate a characteristic parameter for the cell (or figure of merit) called fill factor (FF). The fill factor (FF) is defined as the ratio between the power produced by the cell acting as an ideal cell (P_i) and the maximum power effectively produced by the cell (P_m) (equation 7.2):

$$FF = \frac{P_m}{P_i} = \frac{I_{max}V_{max}}{I_{SC}V_{OC}}. \tag{7.2}$$

At the ideal cell behavior, the I vs V sweep has a square step shape like and the FF is equal to the unity (product between I_{SC} and V_{OC}). For the real cell the resistances induce a sweep with a knee in proximity of V_{OC} and the FF is lower than 1. For that reason the FF is a direct evaluation of the solar cell quality and it is used to control the massive production of solar panel.